AD-A062 851 WESTINGHOUSE DEFENSE AND ELECTRONIC SYSTEMS CENTER B--ETC F/G 20/6
BROADBAND ZINC OXIDE TRANSDUCERS FOR INTEGRATED OPTICS.(U)
JUN 78 D MERGERIAN F33615-77-C-1030
UNCLASSIFIED TRW-78.4734.7-023-PT-2-V0 AFAL-TR-78-92 NL

1 OF 1
AD A062 851

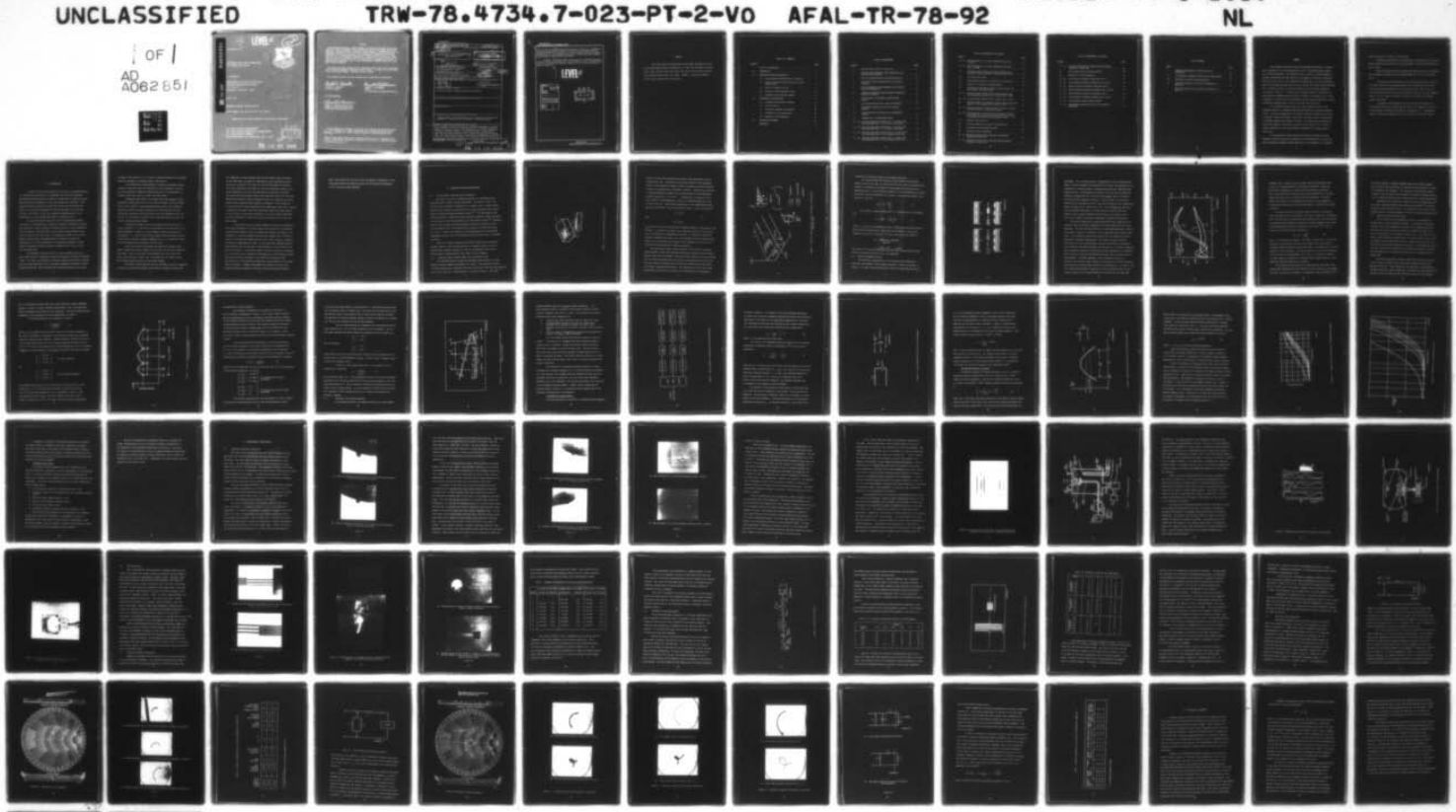

END
DATE FILMED
2-79
DDC

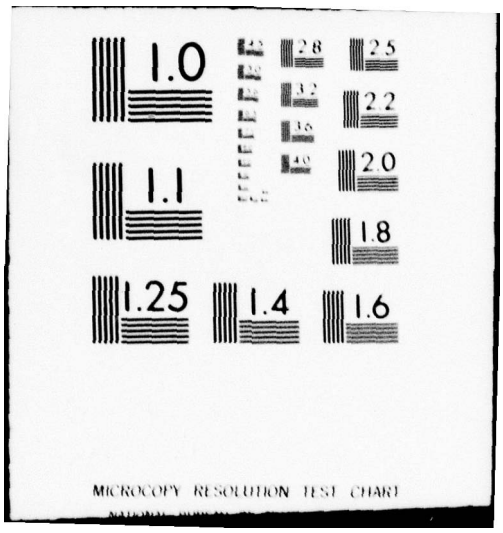
1.0
1.1
1.25
1.4
1.6
2.8
3.2
3.6
4.0
2.5
2.2
2.0
1.8
MICROCOPY RESOLUTION TEST CHART

LEVEL II

AFAL-TR-78-92

BROADBAND ZINC OXIDE TRANSDUCERS FOR INTEGRATED OPTICS

D. Mergerian

Westinghouse Electric Corporation
Systems Development Division
P.O. Box 746
Baltimore, Maryland 21203

June 1978

TECHNICAL REPORT AFAL-TR-78-92

Final Report for Period 4/1/77 to 12/31/77

Approved for public release; distribution unlimited

AIR FORCE AVIONICS LABORATORY
AIR FORCE WRIGHT AERONAUTICAL LABORATORIES
AIR FORCE SYSTEMS COMMAND
WRIGHT-PATTERSON AIR FORCE BASE, OHIO 45433

NOTICE

When Government drawings, specifications, or other data are used for any purpose other than in connection with a definitely related Government procurement operation, the United States Government thereby incurs no responsibility nor any obligation whatsoever; and the fact that the government may have formulated, furnished, or in any way supplied the said drawings, specifications, or other data, is not to be regarded by implication or otherwise as in any manner licensing the holder or any other person or corporation, or conveying any rights or permission to manufacture, use, or sell any patented invention that may in any way be related thereto.

This report has been reviewed by the Information Office (OI) and is releasable to the National Technical Information Service (NTIS). At NTIS, it will be available to the general public, including foreign nations.

This technical report has been reviewed and is approved for publication.

Michael C. Hamilton

MICHAEL C. HAMILTON
Project Engineer

Kenneth R. Hutchinson

KENNETH R. HUTCHINSON
Chief
E-O Techniques and Applications Grp

FOR THE COMMANDER

Ronald F. Paulson

RONALD F. PAULSON, Acting Chief
Electro-Optics Technology Branch
Electronic Technology Division

"If your address has changed, if you wish to be removed from our mailing list, or if the addressee is no longer employed by your organization please notify AFAL/DHO-2 ,W-PAFB, OH 45433 to help us maintain a current mailing list".

Copies of this report should not be returned unless return is required by security considerations, contractual obligations, or notice on a specific document.

UNCLASSIFIED

SECURITY CLASSIFICATION OF THIS PAGE (When Data Entered)

REPORT DOCUMENTATION PAGE

READ INSTRUCTIONS BEFORE COMPLETING FORM

1. REPORT NUMBER: AFAL-TR-78-92	2. GOVT ACCESSION NO.
3. RECIPIENT'S CATALOG NUMBER	
4. TITLE (and Subtitle): BROADBAND ZINC OXIDE TRANSDUCERS FOR INTEGRATED OPTICS	5. TYPE OF REPORT & PERIOD COVERED: Final Technical Report, 1 April [illegible] to 31 Dec [illegible] 77
	6. PERFORMING ORG. REPORT NUMBER
7. AUTHOR(s): D. Mergerian	8. CONTRACT OR GRANT NUMBER(s): F33615-77-C-1030 new
9. PERFORMING ORGANIZATION NAME AND ADDRESS: Westinghouse Electric Corporation, Systems Development Division, P. O. Box 746, Baltimore, Maryland 21203	10. PROGRAM ELEMENT, PROJECT, TASK AREA & WORK UNIT NUMBERS: Program Element, 62204F, Project 2001 02/52
11. CONTROLLING OFFICE NAME AND ADDRESS: Air Force Avionics Laboratory (AFAL/DHO), Air Force Wright Aeronautical Laboratories, AFSC, Wright Patterson AFB, Ohio 45433	12. REPORT DATE: June [illegible] 78
	13. NUMBER OF PAGES: 82
14. MONITORING AGENCY NAME & ADDRESS (if different from Controlling Office): 83p.	15. SECURITY CLASS. (of this report): Unclassified
	15a. DECLASSIFICATION/DOWNGRADING SCHEDULE

16. DISTRIBUTION STATEMENT (of this Report)

Approved for public release; distribution unlimited

17. DISTRIBUTION STATEMENT (of the abstract entered in Block 20, if different from Report)

18. SUPPLEMENTARY NOTES

19. KEY WORDS (Continue on reverse side if necessary and identify by block number)

Integrated optics, spectrum analyzer, ZnO, piezoelectric, acousto-optic transducers, transducer matching networks, rf spectrum analysis

20. ABSTRACT (Continue on reverse side if necessary and identify by block number)

This program involved the design and subsequent development of acousto-optic transducers on silicon substrates for use in integrated optical systems for rf spectrum analysis. The transducers were to cover a minimum bandwidth of 250 MHz centered about 400 MHz and were to be capable of achieving transduction losses of 14dB or less at the frequency of minimum loss. Two such transducers were to be designed and fabricated, one for use with 7059 Corning glass waveguides with a refractive index of 1.58 and the

DD FORM 1 JAN 73 1473 EDITION OF 1 NOV 65 IS OBSOLETE

UNCLASSIFIED

SECURITY CLASSIFICATION OF THIS PAGE (When Data Entered)

405 897

78 12 28 020

other for use with Nb_2O_5 waveguides of refractive index 2.10. In addition, the program called for the design and fabrication of broadband matching networks to match the transducers to a 50-ohm transmission line and permit the adjustment of phase between transducers in order to provide a response which is flat to 2 dB over the entire band.

Measured transduction losses of less than the 14 dB goal have been obtained, however, the propagation losses measured in both the piezoelectric ZnO and in the waveguide layer rule against the use of such transducers at higher frequencies.

LEVEL II

PREFACE

This final report was submitted by the Systems Development Division of the Westinghouse Electric Corporation, P.O. Box 1521, Baltimore, Maryland 21203, under contract F33615-77-C-1030, with the Air Force Avionics Laboratory, Wright-Patterson AFB, Ohio 45433. Michael C. Hamilton, AFAL/DHO, is the Project Engineer for this project.

TABLE OF CONTENTS

LIST OF ILLUSTRATIONS

LIST OF ILLUSTRATIONS (continued)

LIST OF ILLUSTRATIONS (continued)

LIST OF TABLES

SUMMARY

This program involved the design and subsequent development of acousto-optic transducers on silicon substrates for use in integrated optical systems for rf spectrum analysis. The transducers were to cover a minimum bandwidth of 250 MHz centered about 400 MHz and were to be capable of achieving transduction losses of 14 dB or less at the frequency of minimum loss. Two such transducers were to be designed and fabricated, one for use with 7059 Corning glass waveguides with a refractive index of 1.58 and the other for use with Nb_2O_5 waveguides of refractive index 2.10. In addition, the program called for the design and fabrication of broadband matching networks to match the transducers to a 50-ohm transmission line and permit the adjustment of phase between transducers in order to provide a response which is flat to 2 dB over the entire band.

The transducer design consists of a three element array with each transducer having 2.5 interdigital periods and covering a fractional bandwidth of 24%. The center frequencies of the three individual transducers are located at 300 MHz, 382 MHz and 487 MHz, and the array provides a total 3 dB bandwidth of 282 MHz extending from 264 MHz to 546 MHz. The individual transducers are tilted with respect to each other by angles of the order of 0.15° in order to insure satisfaction of the Bragg condition throughout the frequency band of each device.

The configuration chosen because it provides the greatest electro-mechanical coupling involves the deposition of the piezoelectric ZnO film over the interdigital transducer fingers which are in turn deposited on a thermally

grown SiO_2 layer on a (100) cut silicon wafer.

Transducers fabricated in this manner have been measured to have transduction losses which are as low as 6 dB at 480 MHz, 7.5 dB at 380 MHz and 10.5 dB at 320 MHz.

Matching networks have been designed and fabricated which successfully map a transducer impedance with an unmatched VSWR of 40:1 into a 2.5:1 VSWR circle.

Two wafers were fabricated which yield significantly better transduction efficiencies than the remaining wafers, and it appears that the yield on such high quality transducers is of the order of 10%. Most of the ZnO films produced are optically clear and uniform in thickness over the transducer region. A 179.9° taper is provided to launch the wave onto the waveguide region of the wafer.

Propagation loss measurements using laser probing techniques at two different facilities indicate that the loss in the piezoelectric material is of the order of 40 dB/cm at 290 MHz and increases as f^2. Corresponding losses in 7059 glass waveguides fall in the range of 4-7 dB/cm at 290 MHz.

1.0 INTRODUCTION

In order to allow the utilization of silicon as a substrate material in integrated optical devices it is essential that thin film transducer technology be developed which will permit the fabrication of efficient broadband acousto-optic transducers on this non-piezoelectric substrate. This program involved the design and fabrication of two such thin film transducers, to be used with waveguides of 7059 Corning glass in one case and of Nb_2O_5 in the other, to serve as a feasibility demonstration of the applicability of silicon-based technology to integrated optics.

The specific problem areas which were to be addressed included: the design of a transducer array capable of providing a bandwidth of greater than 250 MHz at a center frequency of 400 MHz using ZnO as the piezoelectric thin film material; the fabrication of such arrays showing measured transduction losses of less than 14 dB at the frequency of lowest loss; and the design and fabrication of broadband matching networks that match the transducers to a 50 ohm transmission line and permit adjustment of phase between transducers in order to provide a response which is flat to 2 dB over the entire band.

The transducer design consists of a three transducer array with each device having 2.5 interdigital periods and covering a fractional bandwidth of 24%. The total 3 dB bandwidth of the array extends from 264 MHz to 546 MHz with the center frequencies of the individual transducers located at 300 MHz, 382 MHz and 487 MHz. The transducers are tilted with respect to each other

by angles of the order of 0.15° in order to insure satisfaction of the Bragg condition throughout the frequency band of each device.

The configuration chosen because it provides the greatest electromechanical coupling involves the deposition of the piezoelectric ZnO film over the interdigital transducer fingers which are in turn deposited on a thermally grown SiO_2 layer on a (100) cut silicon wafer.

Transducers fabricated in this manner have been measured to have transduction losses which are as low as 6 dB at 480 MHz, 7.5 dB at 380 MHz, and 10.5 dB at 320 MHz. These measurements were made by using identical transducers located 5 mm apart to measure the total insertion loss and subsequently subtracting the bidirectional loss, the propagation loss, and that part of the mismatch loss which can be recovered through the use of a suitably designed matching network.

The matching network utilizes two elements when the electrical Q of the transducer, i.e., the ratio of the imaginary to the real part of the complex impedance, is small; but three element networks are necessary in cases where $Q > 4$. The use of such three element networks has been found to be sufficient to map the transducer impedance into a 2.5:1 VSWR circle when the initial VSWR before matching was as high as 40:1.

During the course of the program two wafers were produced which exhibit significantly lower transduction loss than the other more representative wafers. One of these wafers also exhibited very high Q values and was the most difficult to match, but it provided the best overall results after suitable matching using a three element network.

The overall results indicate that ZnO technology on silicon substrates is capable of providing transducers which exhibit transduction losses that

are comparable to those achieved using the more simple $LiNbO_3$ technology. On the other hand, the yields in fabrication of such high-quality transducers are at present of the order of only 10% and attempts to identify the better transducers on the basis of electron diffraction results or the visual appearance of the ZnO film have been only moderately successful. Those ZnO films which appear cloudy or hazy have been found to be less well-ordered than perfectly uniform transparent films, but uniformity and transparency do not guarantee good transducer performance. Thus, although all of the ZnO films for which transduction loss measurements are given in Section 3 appeared to be equally clear and uniform upon inspection either visually or via the use of a high power microscope, only a few yielded sufficiently efficient transduction to meet the 14 dB loss criterion set as a goal for this program.

A discrepancy exists at present between the excellent transduction efficiencies measured on the better wafers and the values of k^2 determined using measured impedance values to estimate the radiation resistance of the transducers. The good transduction efficiencies suggest that k^2 should be close to its theoretical maximum value of 0.027, which requires a radiation resistance of approximately 48 ohms. On the other hand, impedance measurements indicate that the real part of the resistance is only 59 ohms on the best of the wafers. If we assume a model in which the radiation resistance, R_a, is in series with a dissipative resistance due to the transducer fingers and calculate the DC resistance of the 1600 Å thick fingers, we find that nearly all of the measured 59 ohms would be accounted for by this dissipative resistance. Impedance measurements at frequencies of twice the acoustic resonance frequencies, where the radiation resistance should be

small, also confirm that the bulk of the resistance is dissipative. This discrepancy between the measured results and the theoretical dependence of k^2 on R_a has not been explained.

2.0 TRANSDUCER DESIGN CONSIDERATIONS

2.1 Silicon Based Integrated Optics Technology

The use of silicon as a substrate material for integrated optical waveguides offers several distinct advantages. The material itself is of low cost and is available in diameters of 3 inches or more. Recent results indicate that high quality sputtered glass or Nb_2O_5 waveguides can be fabricated to minimize waveguide scattering effects.[1,2] The semiconductor substrate also makes it possible to monolithically incorporate linear photodiode or CCD arrays to which the waveguide can be efficiently coupled.[3,4] Waveguide lenses of the Luneberg variety are possible because the refractive index of the waveguide film is relatively low in the case of 7059 Corning glass ($n = 1.58$). Finally, the prospect of incorporating much of the associated integrated circuitry for the photosensor array on the same wafer is extremely attractive.

The use of silicon substrates does however complicate an integrated optical circuit in that the fabrication of a transducer array on the non-piezoelectric substrate requires the use of a piezoelectric film such as ZnO to launch a surface acoustic wave (SAW) into the waveguide.

2.2 Launching Surface Acoustic Waves with Interdigital Grids

The preferred method of generating Rayleigh surface waves on a piezoelectric material employs interdigital (ID) grids.[5] One possible structure, in which the ZnO film is deposited over the ID grid which itself has been deposited on a film of SiO_2 on a silicon substrate, is shown in Figure 1. The lower

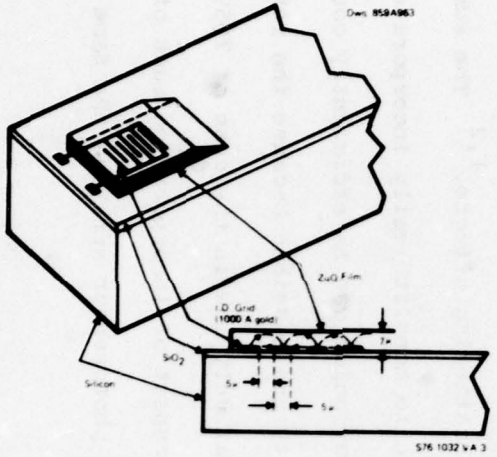

Figure 1 ZnO Film with ID Grid on SiO_2 on Si

portion of this figure indicates the electric field distribution in the piezoelectric film. The manner in which these electric field components couple to the piezoelectric moduli of ZnO to generate the strains required to launch a Rayleigh wave is indicated in Figure 2, where the X_1 direction is selected arbitrarily because ZnO is piezoelectrically and elastically isotropic about the X_3 (or Z) axis. By applying an rf signal to the ID grid, electric field components E_1 and E_3 are generated along the X_1 and X_3 axes of the ZnO. These couple respectively to the piezoelectric moduli d_{31} and d_{15} and result in the Rayleigh wave strains ε_1 and ε_5 given by [6]

$$\varepsilon_1 = d_{31} E_3$$

and (1)

$$\varepsilon_5 = d_{15} E_1$$

ε_5 gives rise to the shear displacement component normal to the surface of the ZnO while ε_1 produces the compressional component parallel to this surface and in the direction of propagation of the SAW. In addition to these displacement components which give rise to the Rayleigh wave, bulk compressional waves are also generated by the electric field component E_3 by virtue of its coupling with the piezoelectric moduli d_{32} and d_{33}.

The piezoelectric matrix shown in Figure 2 can be used to determine crystallographic planes and directions along which piezoelectrically-coupled Rayleigh waves can be launched.[5] When one of these latter directions coincides with an elastic pure-mode direction for both the compressional and the relevant shear modes, piezoelectrically-coupled pure Rayleigh waves can readily be launched, propagated and detected. The piezoelectric matrix also yields piezoelectric surfaces for the material for determining the piezoelectric

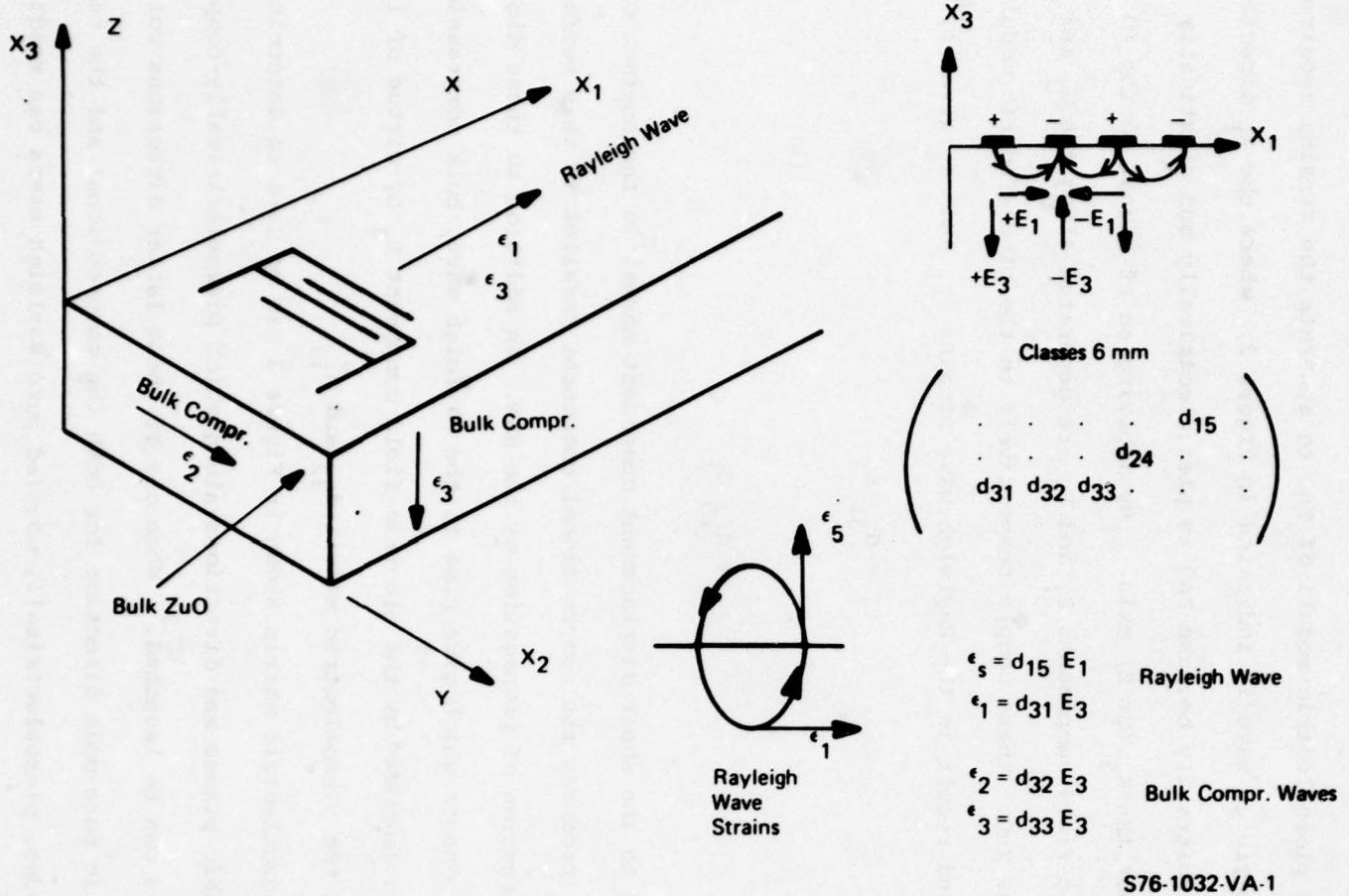

Figure 2 Electric Field Coupling, Strain Generation, and Rayleigh Wave Launching

properties in directions other than pure-mode directions.

In a similar manner the dielectric matrix defines the dielectric surface, which can be used, in conjunction with the elastic and piezoelectric surfaces, to estimate the strength of electromechanical coupling in any desired direction. The relationship between k, the electromechanical coupling coefficient, and the piezoelectric d, elastic C, and dielectric moduli ξ for bulk ZnO is given by

$$k_{ij}^2 = C_{ij} \frac{d_{ij}^2}{\xi_i} \qquad (2)$$

The intrinsic coupling coefficient for a Rayleigh wave can be defined by[7]

$$k^2 = \frac{2\Delta V}{V} = 2 \frac{V_\infty - V_o}{V_o} \qquad (3)$$

where V_∞ and V_o are the piezoelectrically stiffened and unstiffened surface wave velocities respectively. Using published values[8] of V_∞ and V_o, the theoretical intrinsic value of k^2 for a ZnO single crystal half space is

$$k^2 = \frac{2(2681.229 - 2668.198)}{2668.198}$$

$$= 9.7676 \times 10^{-3} = 0.0098\%$$

This value of k^2 can be considerably increased when layered structures such as ZnO on oxidized silicon on silicon are employed.[9]

2.3 Types of Transducer Arrays

Four different configurations of ID electrodes and piezoelectric films have been studied in such layered structures. These are depicted in Figure 3. In Figure 3a the piezoelectric ZnO film is deposited over the ID

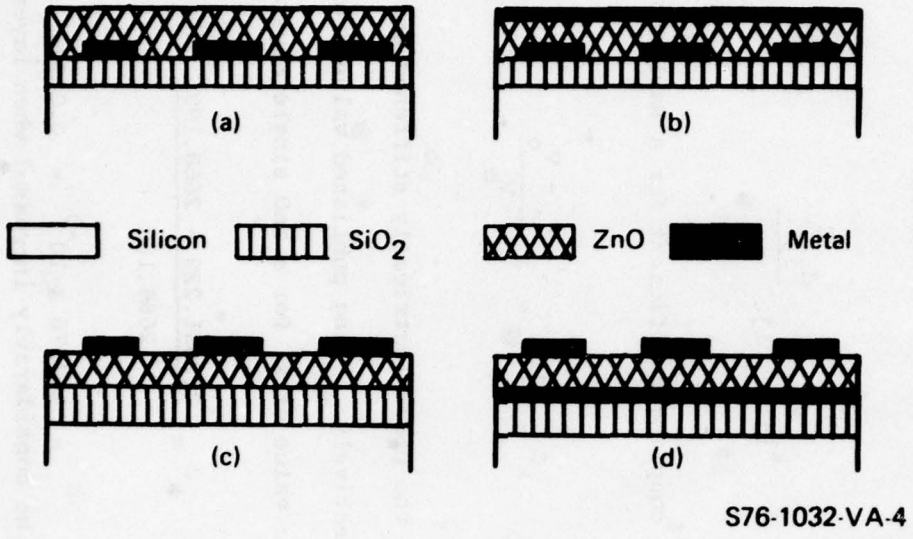

Figure 3 Four ID Configurations for Layered Structures

electrodes. In 3b a shorting plane is deposited over the 3a configuration. Figure 3c and 3d represent the cases where the ID grids are deposited on the piezoelectric film both without a shorting plane and with a shorting plane beneath the ZnO. Solie[9] studied the variation of k^2 for each of these four different configurations as a function of the product (hk) of film thickness and acoustic propagation constant. Figure 4 shows his results and indicates that a maximum value of $k^2 = .028$ was achieved for the configuration shown in Figure 3a for a value of hk = 2.9. This configuration, which has the ID electrodes deposited on a silicon dioxide film and a ZnO piezoelectric film of proper thickness over the grids, can be seen to be the one which is capable of producing the greatest transduction efficiency.

The overall bandwidth of a guided-wave acousto-optic Bragg device is limited by both the acoustic bandwidth of the SAW transducer and the Bragg bandwidth. The first inherent limitation of guided-wave acousto-optic devices which employ a single ID transducer is their relatively small acoustic bandwidth. This limitation results from the fact that the fractional acoustic bandwidth is inversely proportional to the number of finger electrode pairs while the electric-to-acoustic conversion efficiency is proportional to the square of the number of finger electrode pairs. It follows, therefore, that a compromise between the fractional acoustic bandwidth of the transducer and its electric-to-acoustic conversion efficiency sets an overall limit on the bandwidth. The Bragg bandwidth of such guided-wave devices is limited by the acoustic center frequency, the aperture of the SAW transducer, and the optical waveguide modes involved in the diffraction. In order to permit a large Bragg bandwidth (assuming an acoustic bandwidth which is sufficiently larger than the Bragg bandwidth) the aperture of the single SAW

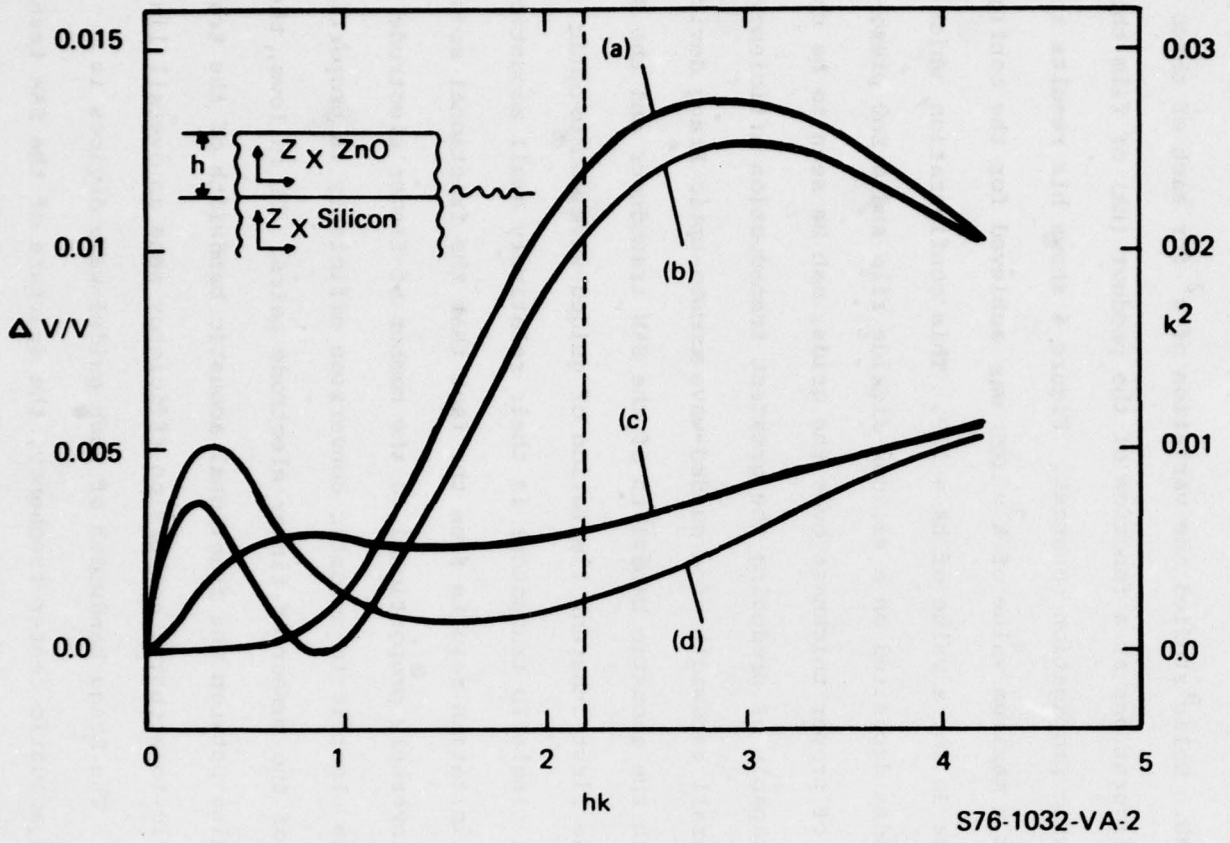

Figure 4 $\Delta V/V$ and k^2 for a ZX ZnO Film on a ZX Silicon Substrate

transducer must be chosen to be very small; and this requirement leads, in turn, to a drastic decrease in diffraction efficiency. Under such unfavorable circumstances, a large rf drive power must be provided if both a large diffraction efficiency and a large bandwidth are to be realized, and this may result in failure of the ID transducer. For these reasons, the product of the diffraction efficiency and the bandwidth of a guided wave acousto-optical device which employs a single SAW is extremely limited.

In order to relieve the aforementioned limitations, two separate device configurations may be employed. The first of these device configurations utilizes multiple interdigital SAW transducers which are characterized by staggered center frequencies and which have their propagation axes tilted through predetermined angles with respect to each other.[10,11] The tilt angles are selected such that the Bragg law

$$\sin \theta_B = \frac{\lambda f}{2nV_s} \qquad (4)$$

where λ is the optical wavelength, n the index of refraction, f the acoustic frequency, V_s the acoustic velocity in the medium, and θ_B the angle of incidence between the optical and acoustic beams, is satisfied for the center frequency of each transducer. By proper selection of the center frequencies and tilt angles of the transducers in an array it is possible to satisfy the Bragg condition throughout the frequency band, thereby enabling a broad composite frequency response to be realized.

The second device configuration is characterized by multiple interdigital SAW transducers which have identical center frequencies and propagation axes, but which are arranged in a staggered or step configuration.[12,13]

The steps introduce a frequency-dependent phase shift between adjacent pairs of SAW's, and this results in a variation in the direction of acoustic propagation with frequency. This scanning of the wavefront enables a composite acoustic beam of large aperture to satisfy the Bragg condition (Eq. 4), thereby allowing efficient diffraction over a wide frequency band.

Experimental and theoretical studies of both the stepped array and the tilted, frequency-staggered array have been performed,[12,14] and both approaches yield high efficiencies. The statement of work (SOW) for this program, however, allowed development of only the frequency-staggered array.

2.4 Design of Tilted Transducer Array

The SOW called for the transducers to have a 3 dB bandwidth of 250 MHz about a center frequency of 400 MHz. The transducer fabrication procedures were to be compatible with either of two waveguide materials, the first being 7059 Corning glass which has a refractive index of 1.58 and the second Nb_2O_5 with a refractive index of 2.10. The radiation resistance of each individual transducer was to be near 50 ohms so that a matching network could be fabricated to yield a response which varies by less than 2 dB over the entire bandwidth of the device. The transduction loss at its lowest value over the band was to be less than 14 dB and the acoustic power launched into the region outside the ZnO at this frequency was to exceed 5 mW.

The minimum bandwidth of 250 MHz is more than covered by utilizing a three element transducer array whose center frequencies are 487 MHz, 382 MHz and 300 MHz. These transducers have individual 3 dB bandwidths of 118 MHz, 92 MHz and 72 MHz, respectively, to produce an overall bandwidth of 282 MHz covering the band from 264 to 546 MHz. Each of the transducers

has 2.5 interdigital periods which allow a 40% fractional acoustic bandwidth; however, in order to provide a suitable safety margin, only a 24% fractional acoustic bandwidth was utilized for each transducer. The center frequencies and bandwidths of the transducers are shown schematically in Figure 5.

The acoustic aperture of a transducer is given by

$$L = \frac{1.8\, n_{eff}\, V_s^2}{\lambda_o\, f_o^2\, m} \qquad (5)$$

where V_s is the effective acoustic wave velocity in the optical waveguide, λ_o the optical wavelength in free space, m the fractional accousto-optic bandwidth and f_o the acoustic center frequency. Assuming effective refractive indices of 1.50 for 7059 Corning glass and 1.95 for Nb_2O_5 waveguides and SAW velocities of 4.2×10^5 cm/sec for both materials, the acoustic apertures for the individual transducers can be determined to be (frequency increases with subscript number):

$L_1 = 4.58$ mm
$L_2 = 2.81$ mm
$L_3 = 1.70$ mm
} for Nb_2O_5 waveguides

and

$L_1 = 3.54$ mm
$L_2 = 2.13$ mm
$L_3 = 1.32$ mm
} for 7059 glass waveguides

The acoustic wave velocity of 4.2×10^5 cm/sec was selected since it falls between the 3.4×10^5 cm/sec velocity measured in fused silica and the 4.4×10^5 cm/sec value measured in Z cut- X propagation silicon.[8] Since the acoustic velocity in Nb_2O_5 was not available at the time of the design, the same value of 4.2×10^5 cm/sec was also utilized in determining

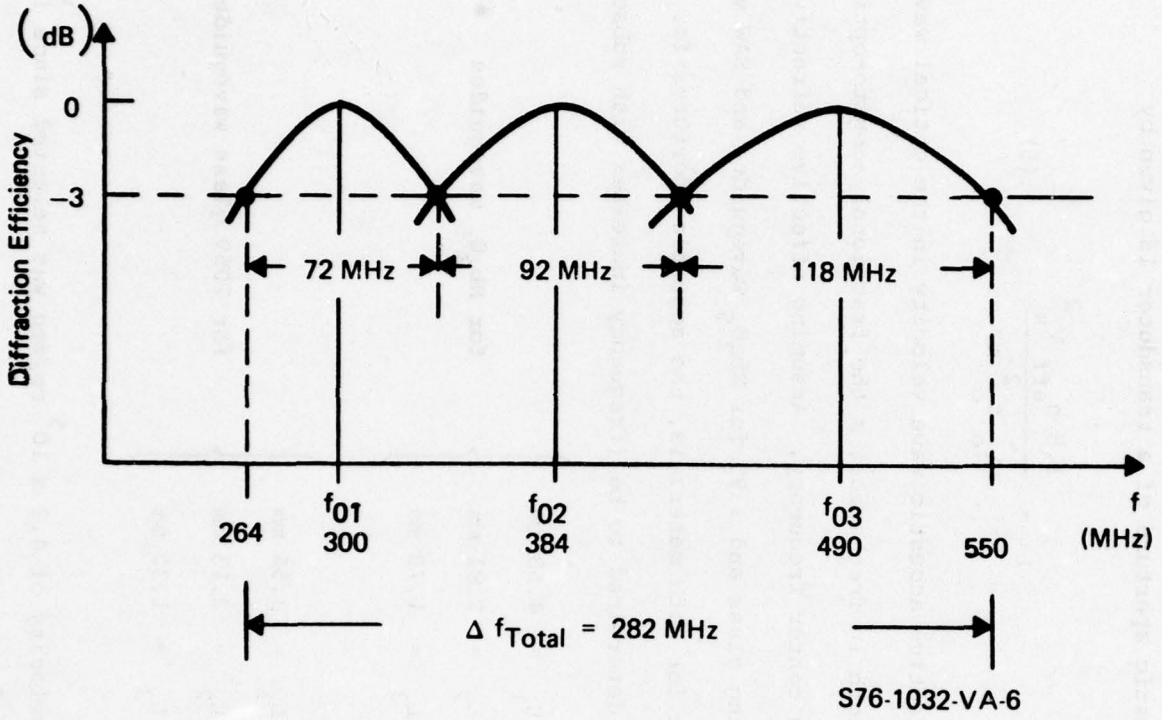

Figure 5 Center Frequencies and Bandwidths for the Three Specified Transducers

the apertures for these transducers.

The transducer configuration was selected on the basis of Solie's studies as summarized in Figure 4. That figure clearly indicates that the configurations with the interdigital electrode structure located at the interface between the ZnO film and the substrate provide the highest electromechanical coupling constants. We ultimately selected configuration (a) which does not utilize a shorting plane over the piezoelectric film as being the better choice of these two because it is simpler to fabricate and it yields a slightly greater value for the electro-mechanical coupling constant.

Having determined the configurations, the center frequencies, and the acoustic apertures, the ZnO film thickness can be determined from $h = 0.5\,\Lambda = 3.23\ \mu m$, where Λ is the acoustic wavelength and we have used $V = 2.58 \times 10^5$ cm/sec for the acoustic velocity for ZnO on oxidized silicon.[15] The theoretical radiation resistance for each of the transducers is given by

$$R_a\,(f_o) = \frac{k^2}{4 f_o (C/L) L} \qquad (6)$$

where C/L is the capacitance per mm per finger pair and k^2 is the electromechanical coupling coefficient. We obtain:

$R_a\,(f_{03}) = 84$ ohms
$R_a\,(f_{02}) = 65$ ohms
$R_a\,(f_{01}) = 51$ ohms
} for transducers with Nb_2O_5 waveguides

$R_a\,(f_{03}) = 110$
$R_a\,(f_{02}) = 85$
$R_a\,(f_{01}) = 67$
} for transducers with 7059 glass waveguides

The radiation resistance for the configuration (b) with a conducting plane over the piezoelectric film is less by approximately a factor

of two than that shown above for configuration (a). This would place the radiation resistances closer to 50 ohms, but it was felt that the stated values were sufficiently close to this figure so that it would not be difficult to design and fabricate an electrical matching network to provide the desired low transduction loss and flat response over the 282 MHz bandwidth.

The tilt angles between the transducers can be determined from the Bragg condition (Eq. 4) at the center frequency of each transducer. For the 7059 glass waveguide the angles between the transducers in the ZnO region are:

$$\phi_{1,2} = 0.15°$$

$$\phi_{2,3} = 0.19°$$

and for the Nb_2O_5

$$\phi_{1,2} = 0.11°$$

$$\phi_{2,3} = 0.14°$$

These values for the tilt angles have been corrected for the refraction of the acoustic wave at the ZnO-waveguide interface. Figure 6 shows a schematic layout of the three transducer array.

Finally, to insure Bragg diffraction, it is necessary that the acousto-optic Q parameter

$$Q = \frac{2\pi\lambda L}{n_{eff}\,\Delta^2} \qquad (7)$$

by sufficiently large (>10). The Q parameters for each of the three transducers designed for use with Nb_2O_5 waveguides are 44 while those designed for the 7059 glass waveguides are 57. We can therefore conclude that Bragg diffraction will prevail in all frequency bands. It is now necessary to adjust the peak diffraction efficiency in each frequency band so as to achieve the necessary flat frequency response.

2.5 Transducer Array Matching Network

As described previously, the approach consists of a three-element

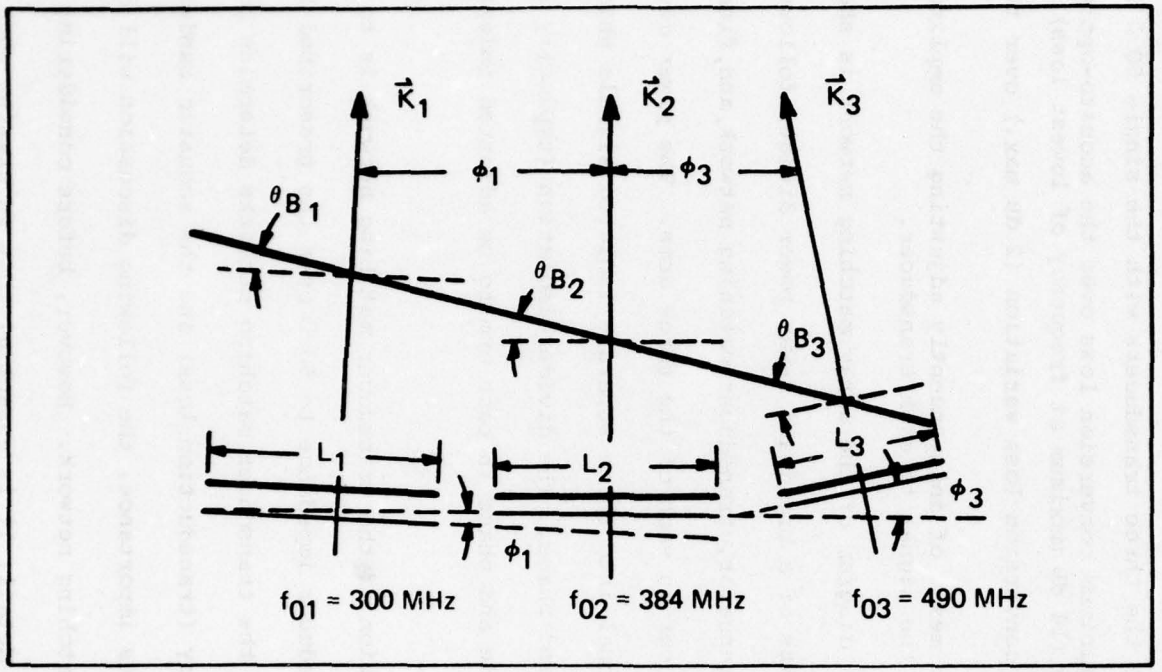

S76-1032-VA-9

Figure 6 Schematic Diagram of Three Specified Transducers Showing Tilt Angles

tilted transducer array with staggered center frequencies. An array matching network is required to efficiently interface the three acoustic transducers with the 50 Ω source. The functions of the array matching network can be summarized as:

a) Interface the three transducers with the single 50 Ω input.

b) Provide minimum conversion loss over the acousto-optic bandwidth (14 dB maximum at frequency of lowest loss).

c) Minimize conversion loss variation (2 dB max.) over the design band.

d) Provide a means of independently adjusting the amplitude and phase of the signal to each transducer.

The block diagram of the array matching network is shown in Figure 7. It consists of a broadband 3-way power divider followed by a phase shifter, attenuator, transducer matching network, and, finally, the acoustic transducer in each of the three arms. The power divider splits the input signal into three separate isolated signals which are equal in amplitude and phase. The divider isolation (typically 25-30 dB) permits the amplitude and phase in each arm to be adjusted independently, without interaction.

The function of the transducer matching network is to match the moderate-Q transducer impedance to 50 Ω over the prescribed bandwidth. To a large measure, the transducer matching networks determine both the conversion efficiency (transduction loss) and the acoustic bandwidth. Therefore, due to its importance, the following discussion will concentrate on the transducer matching network. However, before considering the matching network in detail, it is essential that we examine some of the electrical characteristics of transducers.

Transducer Equivalent Circuit

The series equivalent circuit[10] for an interdigital SAW transducer

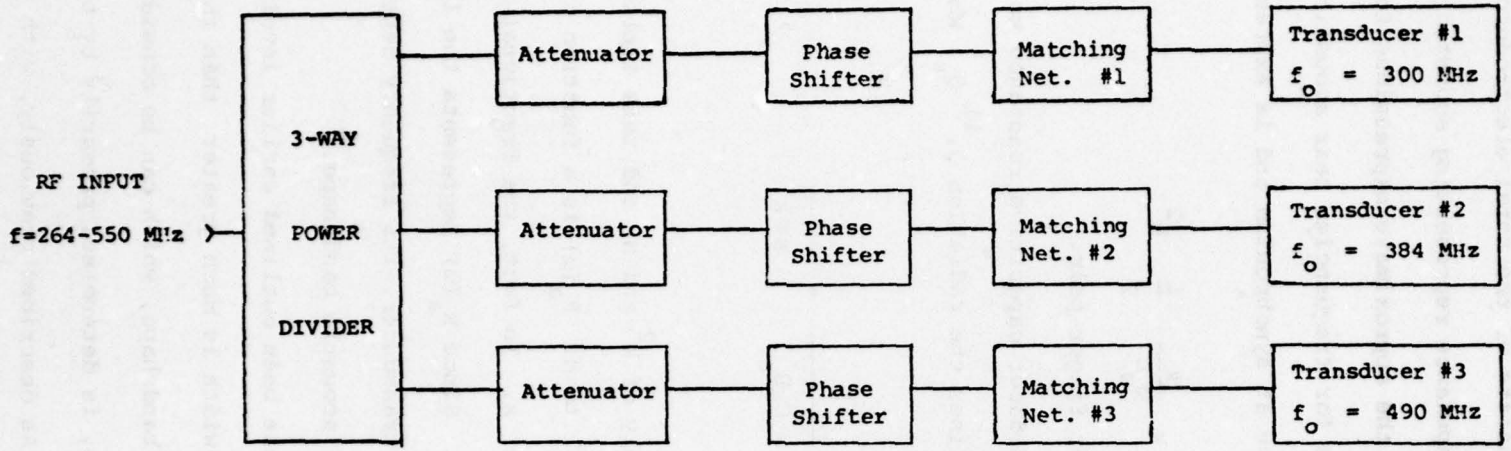

Figure 7 Block Diagram of Transducer Array Matching Network

is shown in Figure 8. It consists of the total electrode capacitance in series with a radiation impedance representing acoustic wave excitation. Also shown in the figure are the approximate expressions for the radiation resistance and reactance for frequencies near acoustic synchronism. $\hat{R}_a$ is the radiation resistance at synchronism and is expressed as

$$\hat{R}_a = \frac{\pi}{\omega_o C} \frac{1}{2} k^2 \tag{8}$$

where C is the capacitance per finger pair.

The ratio of the transducer capacitive reactance to the radiation resistance at synchronism defines the radiation Q,[11] Q_r, which can be expressed as

$$Q_r = \frac{1}{\omega_o C_T \hat{R}_a} = \frac{2}{N\pi k^2} \tag{9}$$

Note that Q_r is a function only of k^2 and N, and this implies an electrical bandwidth that is proportional to N. $R_a(\omega)$ is a function of N through the normalized frequency variable x. In fact, the fractional bandwidth of $R_a(\omega)$ is proportional to 1/N. Since $R_a(\omega)$ represents the flow of acoustic power away from the transducer, its frequency dependence may be regarded as the transducer acoustic bandshape.

The approach, which has been outlined earlier involves selecting N such that the acoustic bandwidth is much greater than the electrical bandwidth. Then the overall bandshape, which can be considered to be the product of the two bandshapes, is determined primarily by the electrical bandwidth and, hence, by Q_r. As described previously, with N equal to 2.5

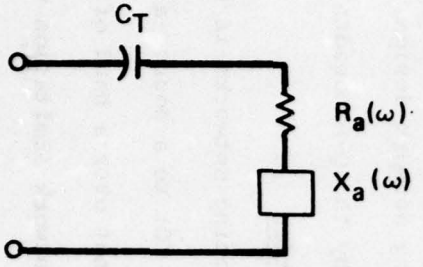

$$R_a(\omega) \cong \hat{R}_a \left(\frac{\sin X}{X} \right)^2$$

$$X_a(\omega) \cong \frac{\hat{R}_a}{X^2} \quad (1/2 \sin 2x - x)$$

$$X = \pi N (\omega - \omega_o) / \omega_o$$

76-1032-VA-28

Figure 8 Series Equivalent Circuit for an ID Transducer

or 3, the corresponding acoustic bandwidth is 40% or 33%, respectively. With an operating bandwidth of 24%, for matching purposes, the transducer may be approximated by an equivalent circuit consisting of a simple series RC network with a constant R. Figure 9 illustrates the approximation for the case of N = 3. $\bar{R}_a$ is chosen to be equal to the geometric mean of the extremes of $R_a(\omega)$ over the design bandwidth. The Q of this series RC circuit with N = 3 and $k^2 = 0.020$ is

$$Q = \frac{1}{\omega_o C_T \bar{R}_a} = 13.26$$

The Q of this equivalent circuit is higher than the radiation Q of the transducer since $\bar{R}_a$ is less than $\hat{R}_a$. The inherent high-Q nature of acoustic transducers results in very definite bandwidth restrictions. Therefore, before considering the actual matching network design, it is appropriate to consider the limitations imposed by the Q-bandwidth product.

The Bode-Fano Network Limitation

An important property of matching networks is that it is possible to perfectly match a complex load ($Q > 0$) to a source at only a finite number of discrete frequencies and not over a band of frequencies. This is a result of the Bode[16] - Fano[17] network limitation which can be expressed as

$$\int_0^\infty \ln \frac{1}{|\Gamma(\omega)|} \, d\omega \leq \frac{\pi \omega_o}{Q} \qquad (10)$$

where $\Gamma(\omega)$ is the input reflection coefficient of the passive lossless network coupling the load to the source and ω_o and Q are the resonant frequency and the Q of the load, respectively. The equality sign holds provided that $\Gamma(\omega)$

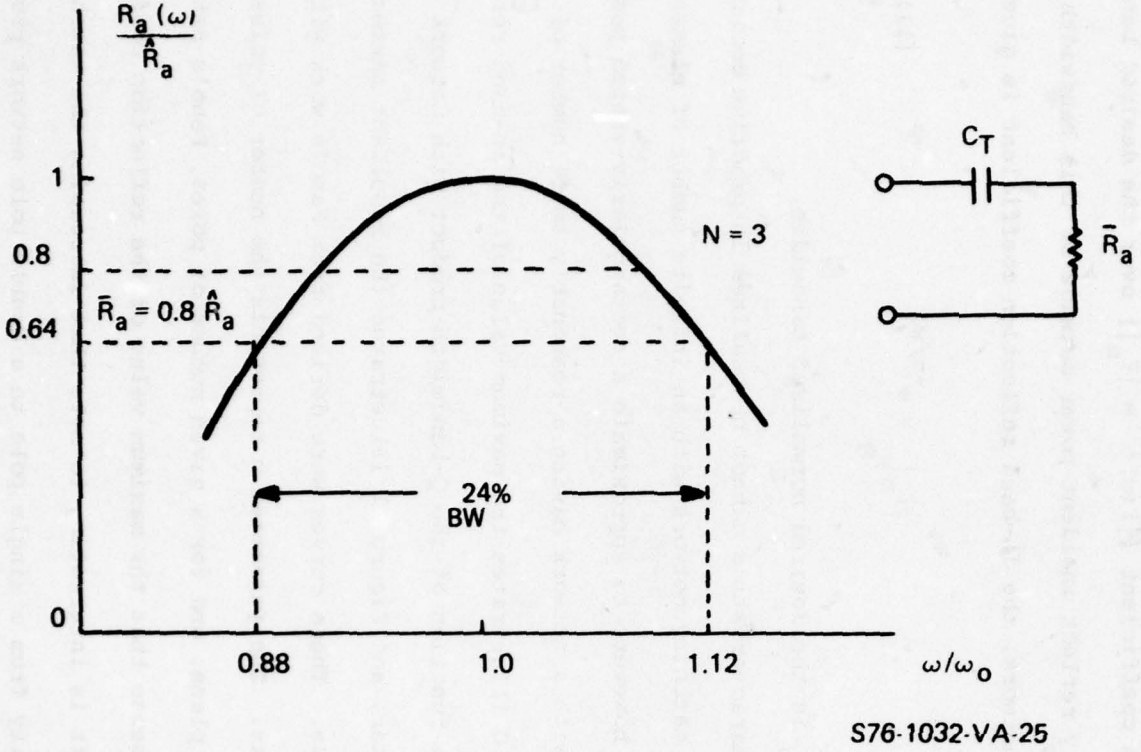

Figure 9 Simplified Equivalent Circuit for Matching Purposes

has no zeros in the right half of the complex plane. This equation illustrates that a low reflection coefficient can be obtained only over a limited bandwidth. In fact the most efficient network would provide a constant input reflection coefficient ($|\Gamma(\omega)| = |\Gamma_m|$) over the desired bandwidth and would totally reflect incident power outside of this bandwidth. For this ideal matching network, the in-band reflection coefficient is given by

$$|\Gamma_m| = e^{-\pi/wQ} \qquad (11)$$

where $w = \Delta\omega/\omega_o$ is the desired normalized bandwidth.

These characteristics cannot be realized in practice because it would require a matching network with an infinite number of elements. It is possible, however, to approximate a rectangularly-shaped passband characteristic with a network having a reasonably small number of elements.

Figure 10 illustrates the maximum value of the in-band reflection coefficient as a function of the Q-bandwidth product with network complexity as a parameter, and Figure 11 illustrates the resultant maximum in-band transmission loss. These curves were derived from Fano's work with lowpass matching networks. The parameter n represents the number of poles in the complex Γ- plane, and for a given number of poles, Fano's network is optimum in the sense that the maximum value of the reflection coefficient is a minimum. It is interesting to note that increasing the matching network complexity from a single pole to a double pole network produces the greatest improvement in the transmission loss, and that little is to be gained for the added circuit complexity beyond n = 3.

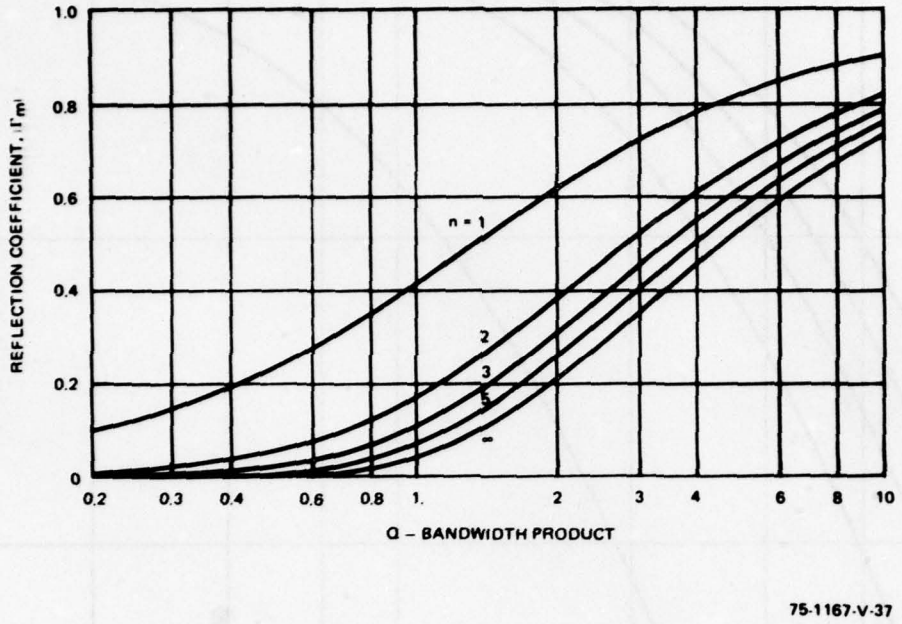

Figure 10 In-Band Reflection Coefficient vs Q-Bandwidth Product

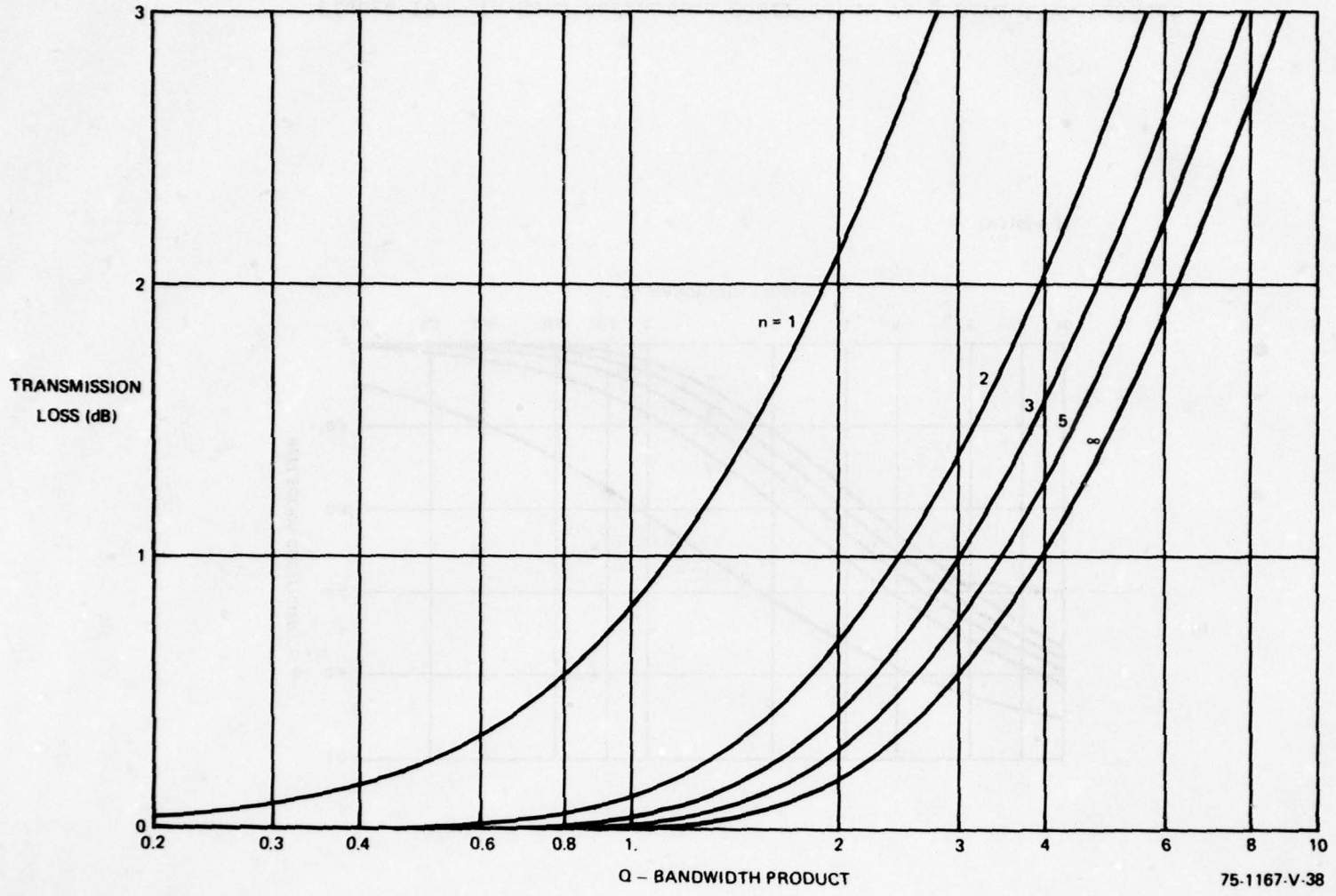

Figure 11 Transmission vs Q-Bandwidth Product

In summary, the purpose of the matching network is to transform the complex load to an impedance locus which represents the minimum reflection coefficient to the source in the frequency band of interest. The ideal matching network would present a reflection coefficient to the source which describes a circle of constant radius, over the desired band, centered at the source impedance.

Transducer Array Losses

Low transduction loss together with "flat" response over the 250 MHz acousto-optic bandwidth are critical requirements of the transducer array. By properly designing the matching networks and adjusting the phases of the transducers, the response variation can be held below the 2 dB requirement. The various sources contributing to the total transduction loss are summarized as:

1) The interdigital transducer's bidirectional loss, 3 dB.
2) Dissipative losses in the transducer and in the transducer matching network.
3) Matching network mismatch losses, 1.5 dB.
4) Losses in the attenuator and phase shifter.
5) 3-way power split loss, 4.8 dB.
6) Dissipative losses in the power splitter (typically 0.7 dB).

The function of the attenuator is the equalization of transducer losses, and it should not, therefore, be considered as a source of transduction loss. The loss in the phase shifter is negligible. Thus, the total transducer loss tally comes to 10 dB plus the dissipative losses in the transducer and in the transducer matching network.

The key to minimization of dissipative loss lies in choosing the number of finger pairs, N, to be as large as possible, provided that it is consistent with the bandwidth requirements of the device. The choice of N equal to 2.5 has been seen to yield an adequate bandwidth safety margin. In addition, we estimate, based on previous experience, that it limits the dissipative loss to less than 2 dB. Consequently, the total transduction loss should be of the order of 12 dB.

3.0 EXPERIMENTAL INVESTIGATIONS

3.1 Transducer Fabrication Technique

The n-type silicon substrates upon which the ZnO transducers were fabricated were purchased from Monsanto and had minimum resistivities of 100 ohm-cm. The wafers were two inches in diameter and were cut in the (100) plane. The wafers were oriented such that the acoustic wave propagation was along the (011) direction. This propagation direction was chosen simply because the "D" cut provided on the wafers could be conveniently utilized during transducer mask alignment. The wafers were ordered with a "mon-x" polish which proved adequate for the fabrication of high quality transducer elements without additional optical polishing.

The wafer processing involved an initial cleaning utilizing standard cleaning procedures employed in the silicon integrated circuits line at the Westinghouse Advanced Technology Laboratories. Following these initial cleaning steps the wafers were rinsed in hot super Q water, dried, and stored in a vacuum dessicator until ready for oxide growth.

The silicon dioxide layers were thermally grown over the entire face of the wafer to a thickness of either 5 μm or 1 μm for subsequent experiments. In addition to experiments performed on thermally grown oxide layers on silicon, silicon dioxide was also formed by sputtering and by the standard SILOX technique. Both of these latter techniques were subsequently rejected because it proved to be impossible to deposit high-quality, well-oriented ZnO films on all but the thermal oxide. Figure 12(a) shows an electron diffraction pattern of a 3 μm thick ZnO film sputtered onto

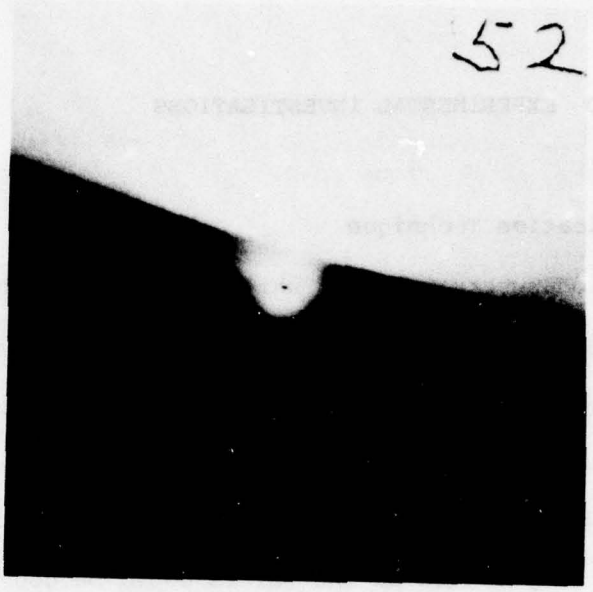

(a) Electron Diffraction Pattern for a 3 μm Thick ZnO Film Sputtered over a 5.4 μm Thick SILOX Layer

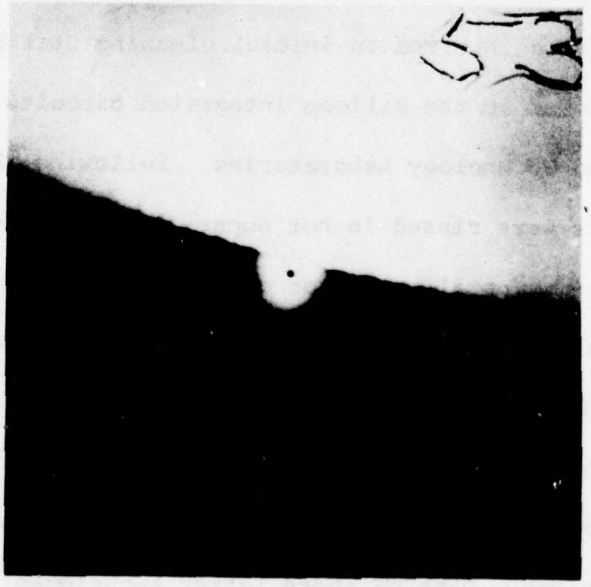

(b) Electron Diffraction Pattern for a 3 μm Thick ZnO Film Sputtered over a < 1 μm Thick SILOX Layer

Figure 12

a 5.4 μm thick oxide film produced by the SILOX growth technique. Figure 12(b) shows the same ZnO film deposited over a portion of the wafer where the SILOX deposition is less than 1 μm thick. The poorer ordering inherent on oxide films produced by this technique is evident upon comparison with the electron diffraction results of Figures 13 (a and b) which were taken for a 3 μm thick ZnO film deposited on 1 μm and 5 μm thermally grown SiO_2, respectively.

In the case of sputtered SiO_2 films, scanning electron microscope studies, Figure 14 (a), compare very favorably, insofar as the film quality is concerned, with that shown in Figures 14 (b) for a thermally grown SiO_2 film. Attempts to deposit ZnO on sputtered SiO_2 films, however, proved unsuccessful. The ZnO films were invariably poorly ordered and were not so clear as were the films sputtered over the thermally grown oxide.

As a result of the inability to sputter well-ordered ZnO films on either SILOX or sputtered SiO_2 films, plans to fabricate transducers on wafers with 1 μm thick thermally grown oxide films in the region of the waveguide and thicker films in the region of the transducers were abandoned. This technique had been considered as one which might combine the advantages of the high quality waveguides formed on 1 μm thick oxide layers with the lower capacitance which would be realized in the transducer region because of the thicker oxide films which would be deposited there. On the other hand, 7059 glass waveguides sputtered over 5 μm thick thermally grown oxide films did not appear to exhibit higher losses than those sputtered over 1 μm oxide films, with losses at that time (6/77) of the order of 2 dB/cm. It was therefore decided to minimize capacitance effects to the substrate by utilizing a 5 μm thick thermally grown oxide film over the entire substrate. These thicker films are grown using a wet process at 1200°C and

(a) Electron Diffraction Pattern for a 3 μm Thick ZnO Film Sputtered over 1 μm of Thermally Grown SiO_2

(b) Electron Diffraction Pattern for a 3 μm Thick ZnO Film Sputtered over 5 μm of Thermally Grown SiO_2

Figure 13

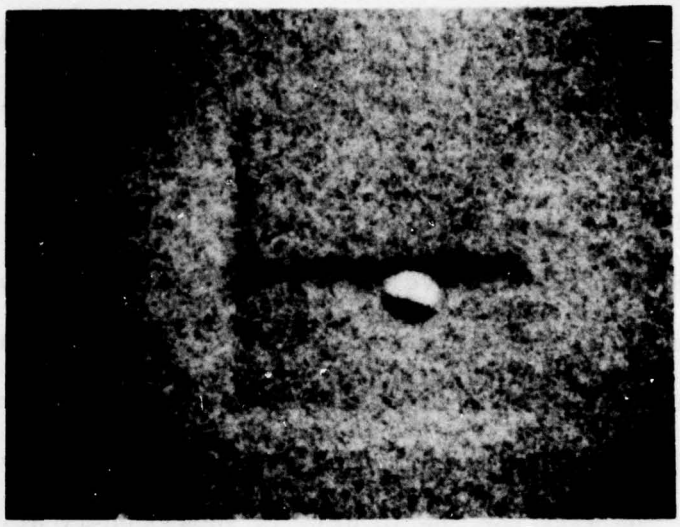

(a) SEM Photograph of 1 μm Thick Sputtered SiO_2 Film - 14,500X

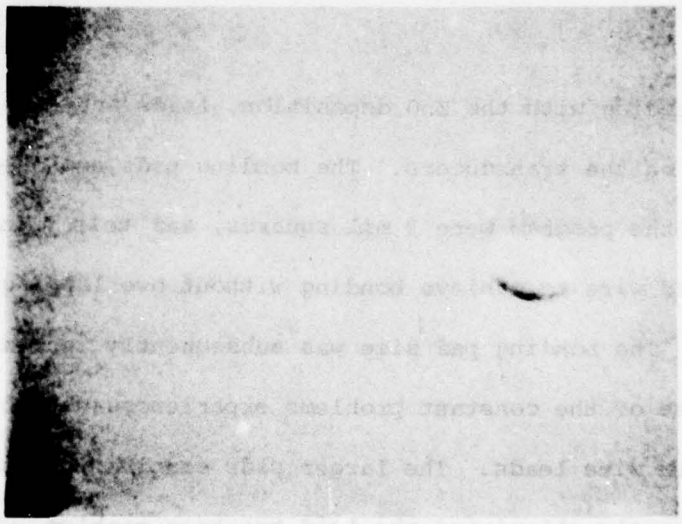

(b) SEM Photograph of 5 μm Thick Thermally Grown SiO_2 Film - 14,500X

Figure 14

require 30 hours of growth.

Following the growth of the 5 μm thick thermal oxide layer, the next step in the fabrication process involves the deposition of the interdigital grids. These electrodes are formed by first evaporating a 50 Å film of chromium followed by an aluminum film to a total thickness of the order of 1600 Å. The wafers are then removed from the evaporator and clamped on a spinner, and photoresist is spun onto the surface of the aluminum film at 2000 rpm for approximately 20 seconds in order to obtain a uniform layer without beads or folds. The wafers are then baked in a vacuum oven for 15 minutes at 90°C. The mask for the ID grid is subsequently aligned on the wafer which is then exposed for 5 seconds to UV radiation. The exposed face is developed, rinsed, dried and etched to remove all aluminum and chromium except in the regions of the ID grids and bonding pads. Following the etching operation the wafers are cleaned in acetone, blown dry and are ready for bonding.

Before proceeding with the ZnO deposition, leads are bonded to each of the bonding pads on the transducers. The bonding pads employed during the early months of the program were 2 mil squares, and this required the use of 0.7 mil diameter gold wire to achieve bonding without overlapping onto the transducer fingers. The bonding pad size was subsequently increased to 4 mil squares because of the constant problems experienced with breaking of the small diameter wire leads. The larger pads enabled the use of 1 mil diameter wire and greatly alleviated the lead breakage problem. The additional capacitance introduced by increasing the area of the bonding pads by a factor of 4 was not significant since the capacitance between the transducer fingers is many times that contributed by the bonding pads.

In all, twelve leads were made to six different transducers on the wafer. All the leads were at first stretched loosely so as not to severely mask the portion of the substrate over which they extended. The opposite ends of these leads were in turn bonded to a special bonding pad, and remained so bonded until after the ZnO deposition. Figure 15 shows the pattern deposited on the substrate, with the leads bonded to the temporary bonding pad. In all, seven transducers are deposited, with the central-most set of three being the ones to be utilized in the acousto-optic experiments. The other set of three transducers is an exact replica of the inner set and is placed 5 mm away so that they may be utilized as receiving transducers in making transduction loss measurements. Finally a single transducer has been placed on the opposite side of the wafer, to act as a receiving transducer to monitor the acoustic beam after it traverses the waveguide region. This transducer is a replica of the intermediate frequency (center) transducer of the array.

The deposition of the 3.2 μm thick ZnO film was accomplished using an rf sputtering technique. Figure 16 shows a generalized schematic of the sputtering set-up employed. The ZnO target is hot-pressed ZnO powder and the deposition of ZnO from the source is uniform over an area of the order of a square inch. The substrates are mounted in a heater-holder and a glass mask is clamped over the substrate to prevent deposition in all regions but those containing the ID grid patterns. The inside edges of the glass mask are beveled so as to create a tapering of the ZnO film in the direction of SAW propagation. Experimental work performed by I.A. Vikrovov[18] on Rayleign waves on dihedral surfaces shows that virtually all of the Rayleigh wave energy is transmitted when the dihedral angle is greater than 170^{o},

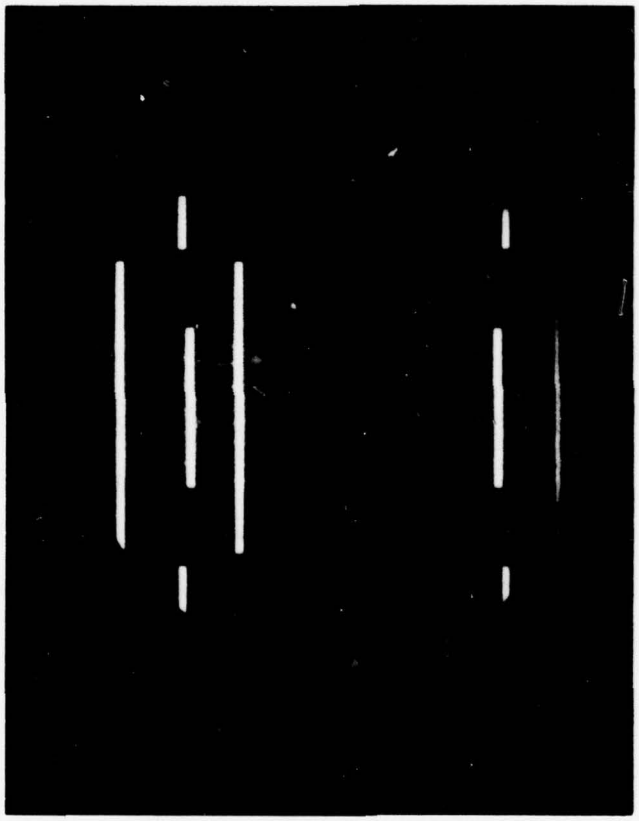

Figure 15 Aluminum Pattern Deposited on SiO_2 Substrates with Transducer Leads Connected to Temporary Bonding Pad

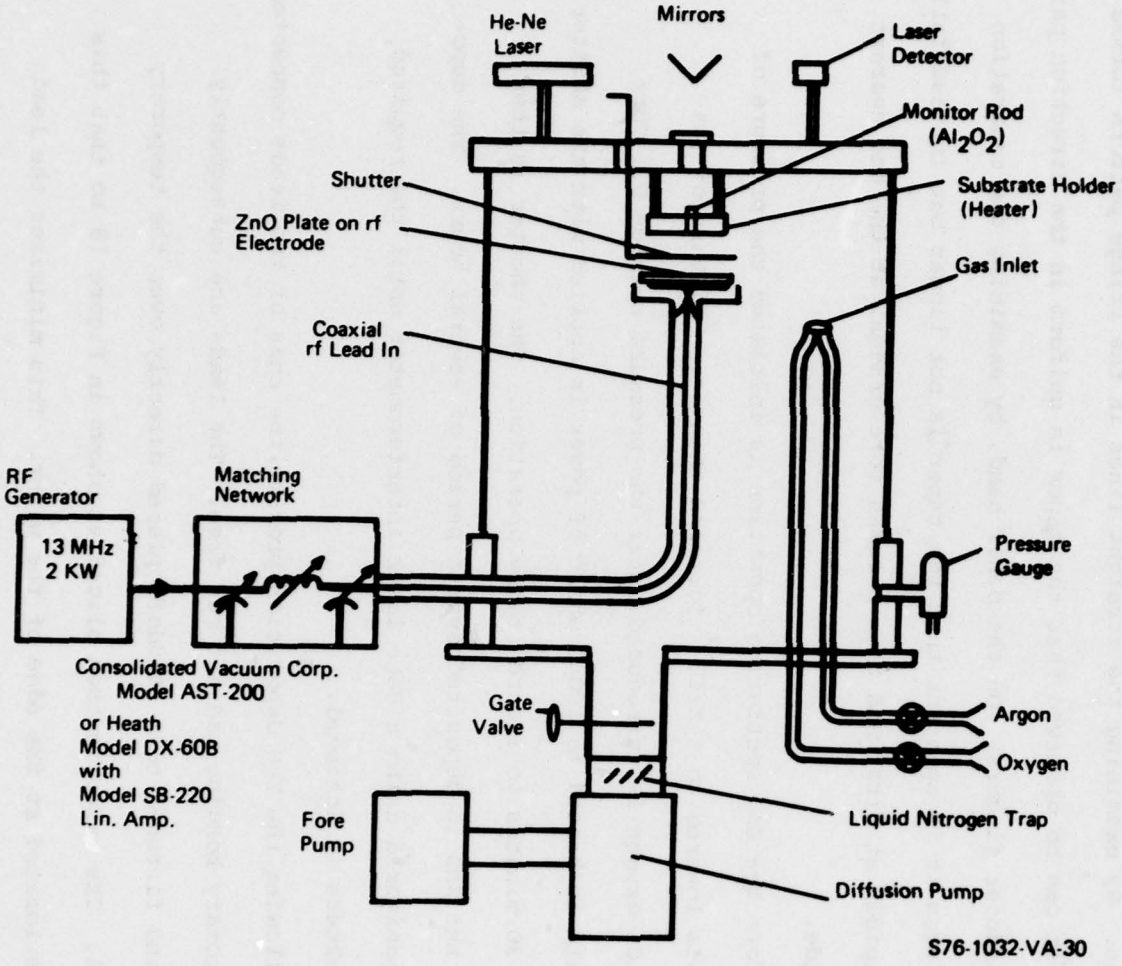

Figure 16 ZnO Sputtering System

see Figure 17. The tapers employed in the transducers produced as part of this program are approximately 2 mm long. For the 3.2 μm film thickness involved this corresponds to a taper angle of 179.9° which should effectively prevent any reflection loss in propagating across the taper into the waveguide region. By examining the straight lines in the fringe pattern formed by this taper it can be observed that the taper is uniform in the direction parallel to the transducer fingers. On the other hand, by examining the separation between fringes it is apparent that the taper is not linear but instead falls off more rapidly at first and then becomes more gradual at the end nearest the waveguide.

Before the ZnO sputtering operation is initiated the pressure of the system is lowered to 5×10^{-7} Torr and then a gas mixture of 90% argon and 10% oxygen is introduced until the pressure reaches 0.1 Torr. The substrate is heated to 100°C while rf power is applied with the shutter closed for 30 minutes to insure stable operation. The shutter is then opened and the ZnO is deposited over a period of several hours. The deposition is monitored using a HeNe laser interferometer until the required 3.2 μm thickness is achieved.

Following the ZnO deposition process, the ends of the leads connected to the temporary bonding pad are cut free. The leads are subsequently shortened and fastened to a standoff placed directly over the temporary bonding pad. The wafer is then sliced as shown in Figure 18 so that this standoff is located at the edge of the wafer. This minimizes the lead lengths from the standoff to the matching network which is subsequently mounted on a separate fixture which butts against the fixture holding the wafer. Figure 19 shows a photograph of this complete assembly with a three element matching network.

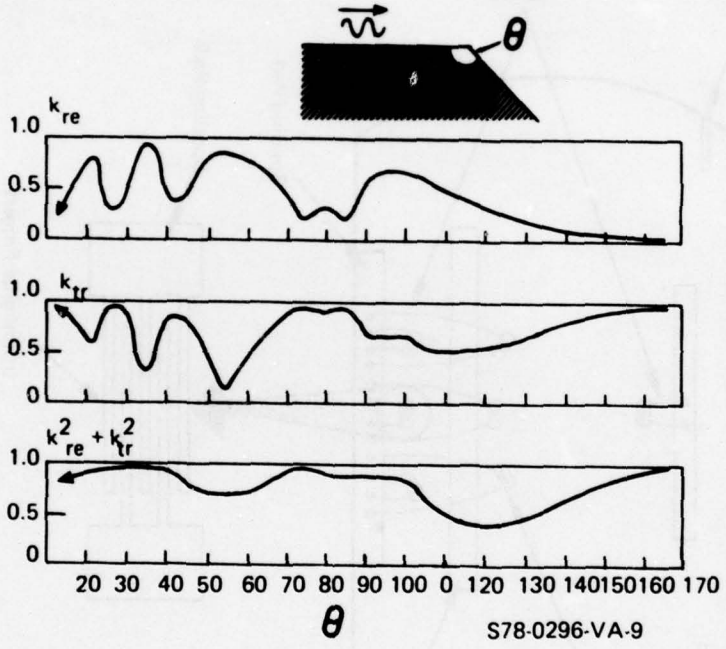

Figure 17 Rayleign Wave Coupling as a Function of Taper Angle

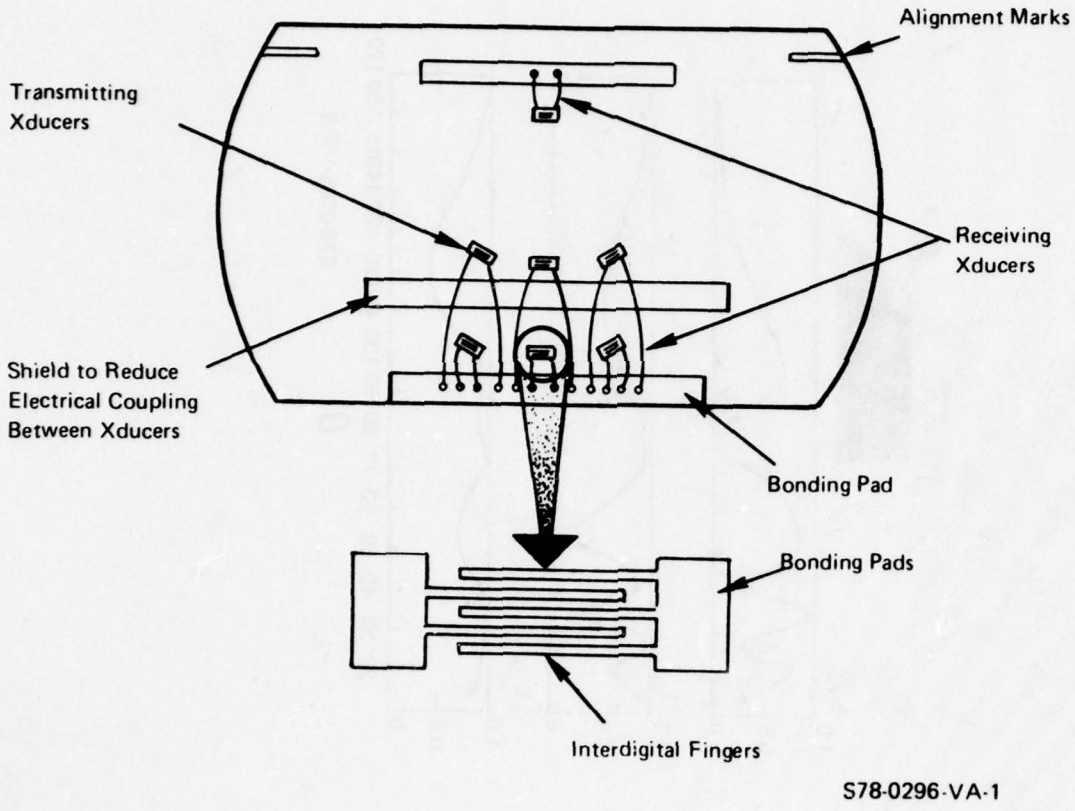

Figure 18 Schematic of Pattern on Completed Wafer

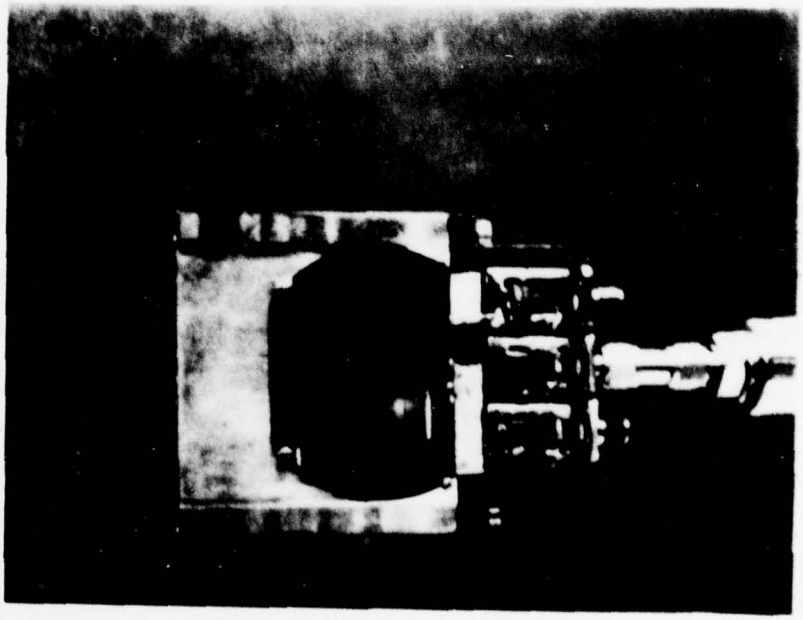

Figure 19 Photograph of Transducer Array on Silicon Wafer with Three Element Matching Network

3.2 ZnO Film Quality

The rf sputtered ZnO films deposited on thermally grown SiO_2 are usually well-ordered with electron diffraction patterns like that shown in the electron diffraction photographs of Figure 13(a&b). Optically, these films can be perfectly clear and of uniform thickness in the region of the transducer array, as shown in Figure 20 (a&b), but this is not always the case. In some instances the deposited films appear milky or hazy and in others we have observed partial lifting of the ZnO or aluminum in the region of the transducer fingers. Figure 21 shows a photomicrograph of a wafer which appeared slightly hazy. This figure also shows a thermal compression ball bonded 0.7 mil diameter lead wire bonded to the 2 mil square bonding pad. Figure 22 (a&b) show transducers in which the ZnO - aluminum has partially lifted in the region of the fingers even though it is clear in the region of the bonding pads. Figure 22 (a) is a 312 X enlargement of the medium frequency transducer (f_o = 38 2 MHz) while Figure 22 (b) shows a similar enlargement of the high frequency transducer (f_o = 489 MHz).

Wafers which exhibited either lifting or haziness were immediately discarded and were not utilized in further testing. All of the wafers on which data are provided in Sections 3.3 and 3.4 were selected using the clearness of the deposited ZnO film and the absence of any lifting of the transducer fingers as criteria. On this basis all of the wafers on which measurements were made appeared equally good; it will be seen in the following sections, however, that the electrical and acoustical properties varied over a considerable range.

3.3 Transducer Impedance Measurement

Impedance measurements were performed prior to electrical matching of the interdigital transducers. Low frequency measurements were made at 264,298 and 336 MHz; mid-range measurements at 336,381 and 432 MHz; and

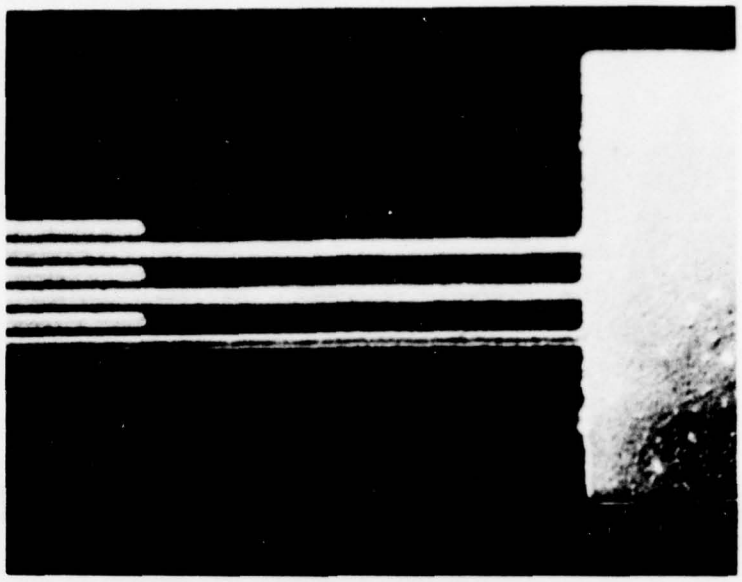

(a) Photomicrograph Showing the Transducer Bonding Pad and Interdigital Fingers Thru 3.2 μm of ZnO - 800X

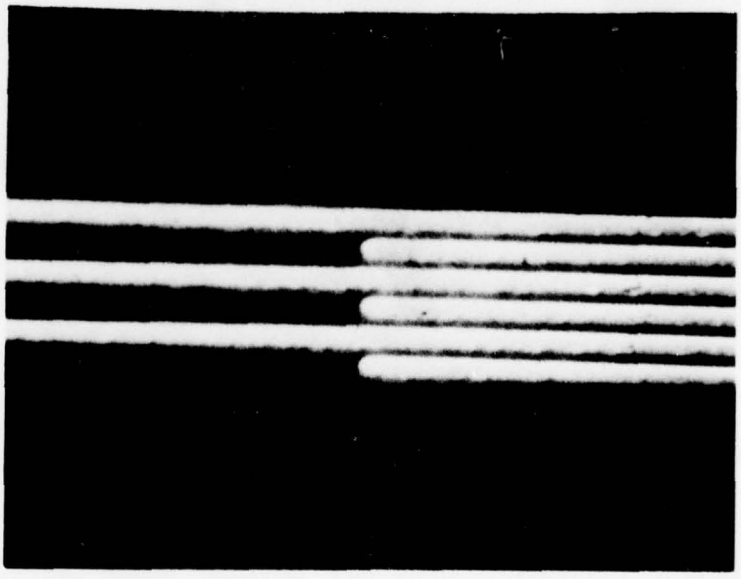

(b) Photomicrograph Showing the ID Fingers Only - 1361X

Figure 20

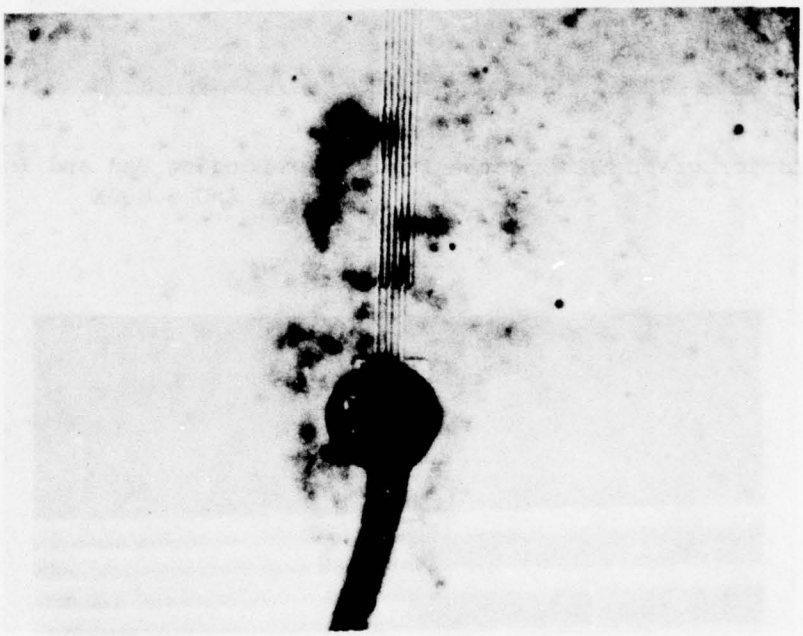

Figure 21 Photomicrograph of Transducer Fingers & Bonding Pad with Bonded 0.7 mil Lead Wire Thru Hazy ZnO Film

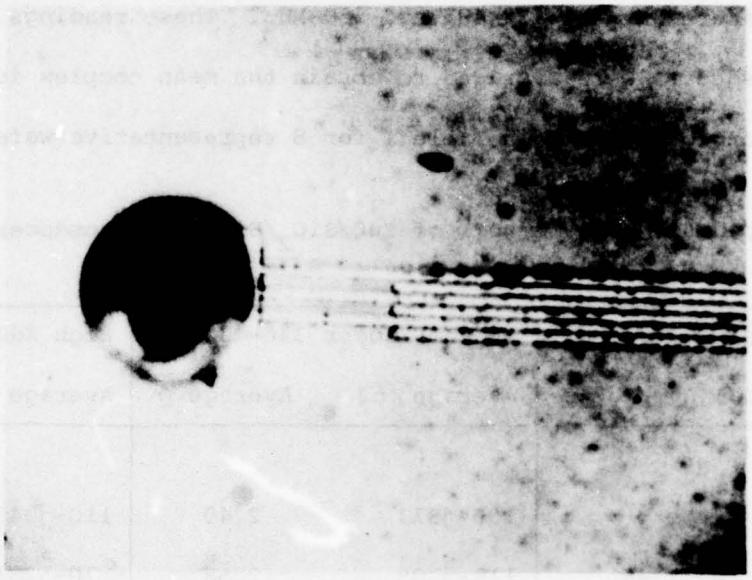

(a) Photomicrograph of Medium Frequency Transducer Showing Lifting of ZnO-Al in Region of Fingers

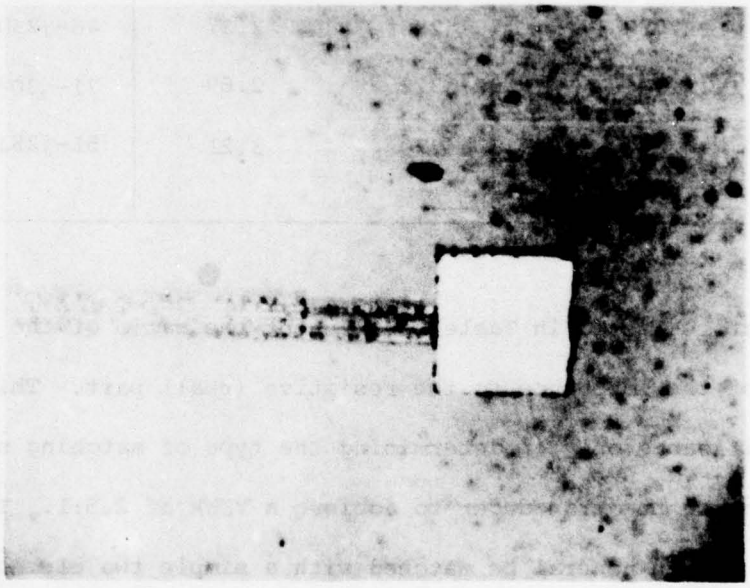

(b) Photomicrograph of High Frequency Transducer Showing Undisturbed ZnO Over Region of Bonding Pad but Lifting Around Edges of Bonding Pad and Around Fingers

Figure 22

high frequency measurements at 432,487 and 550 MHz. These readings on each of the three transducers were averaged to obtain the mean complex impedance which is shown along with the Q in Table I for 8 representative wafers.

Table I Impedance Measurements of ZnO/SiO_2/Silicon Transducers

Wafer#	Low Xducer 264-336MHz		Medium Xducer 336-432MHz		High Xducer 432-550MHz	
	Average Z (Ω)	Average Q	Average Z (Ω)	Average Q	Average Z (Ω)	Average Q
1	-	-	150-j373	2.49	110-j343	3.12
2	166-j240	1.45	118-j305	2.58	70-j283	4.04
3	131-j305	2.33	84-j300	3.57	61-j286	4.69
4	65-j193	2.97	52-j222	4.27	38-j220	5.79
11	59-j250	4.24	52-j261	5.02	28-j238	8.50
13	65-j168	2.58	76-j256	3.37	46-j238	5.17
14	182-j302	1.66	119-j320	2.69	71-j304	4.28
16	112-j285	2.54	87-j279	3.21	51-j253	4.95

The Q factors listed in Table 1 represent the ratio of the reactive (imaginary) part of the impedance to the resistive (real) part. This quotient has significance only in determining the type of matching network to be used in matching the transducer to achieve a VSWR of 2.5:1. The low-Q transducers can in general be matched with a simple two element network while those with higher Q values of 4 or above will require a three element network as discussed in Section 3.5.

These measurements were performed on a network analyzer, but the general location of the impedance curves on a Smith Chart were such that they could not be accurately determined from the polar display of the network analyzer. The return loss and phase shift of each of the transducers were therefore recorded from the network analyzer's rectangular display and converted to complex impedance.

Since the rf connection to the wafers was made via an SMA connector having wire leads running to the transducer bonding pads, an open circuited SMA connector was used as a return loss reference. A negligible amount of inductive reactance due to the bonding wire leads is included in the above impedance results.

3.4 Transduction Loss Measurement

As has been described in Section 3.1, the pattern deposited on the wafer consisted of an identical pair of transducer arrays separated by a distance of 5 mm along the (011) direction of the silicon substrate. The inner array was utilized as a transmitter and the other was used as a receiver. In this manner the total loss in going from electrical input to electrical output was determined.

Because the signal loss observed between the pairs of transducers was so high, a pulsed rf test facility, shown in Figure 23, had to be utilized to measure the insertion loss. The test facility has a dynamic range of 90 dB which is sufficient to allow measurement of all but the most lossy transducer combinations. To begin the measurement, the wafer being tested was emplaced in the circuit, the variable attenuator was set at zero, and the magnitude of the delayed rf pulse was measured on the oscilloscope display. The test sample was then removed and the variable attenuator

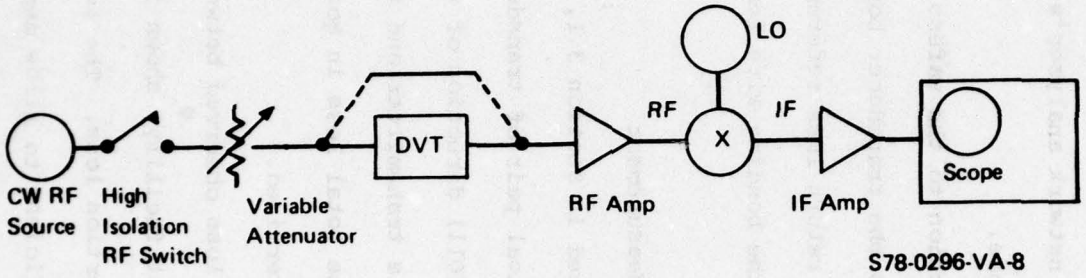

Figure 23 Pulsed rf Test Facility

was turned-up until the pulse height was duplicated, thus providing a direct measure of the overall insertion loss.

The rf pulse response of a typical transducer pair is shown in Figure 24. The initial pulse shown on the left is the result of direct feedthrough of the incident signal caused by mutual coupling of the connecting leads. The second pulse represents the delayed acoustic pulse which would be totally masked by the feedthrough signal if the facility were operated on a swept CW basis as is generally done in a conventional network analyzer.

Insertion loss measurements at five different frequencies on the low frequency transducer of six wafers are shown in Table II. All of these figures were generated without matching the transducer to the input line.

Table II Low Frequency Transducer Insertion Loss Measurements

Frequency MHz	WAFER # #3	#4	#5	#6	#8	#9
260	71	-	92	77	86	86
280	66	-	84	73	81	84
300	64	-	78	68	78	80
320	67	-	78	66	80	79
340	69	75	76	77	81	84

Table III includes the insertion loss measurements taken on the final four wafers which were delivered to the Air Force as part of this program. The insertion loss to the intermediate frequency transducer on wafer #14 could not be measured because of failure of the receiver transducer.

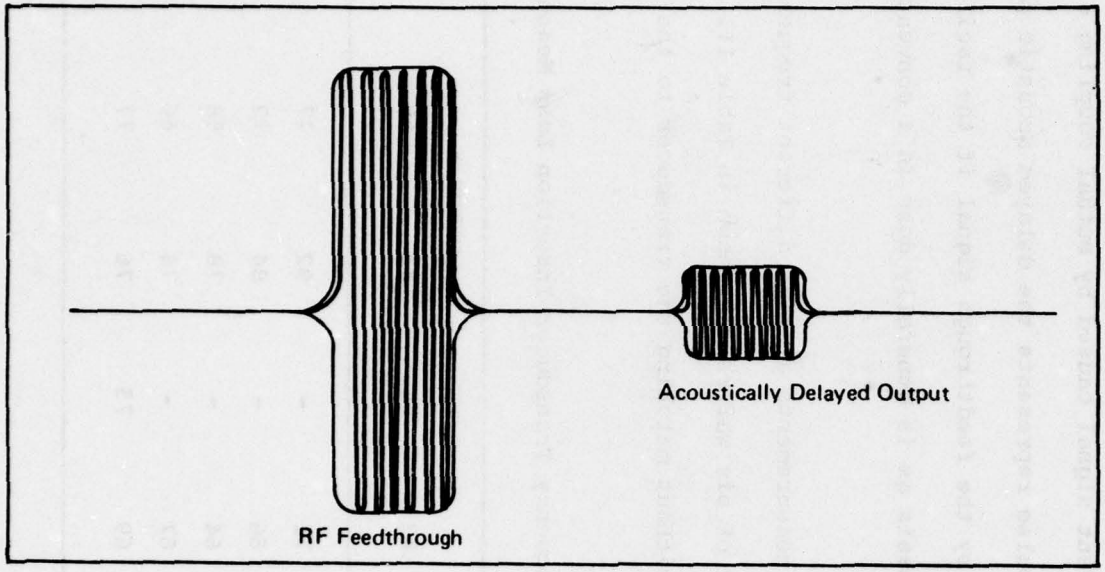

Figure 24 RF Pulse Response of a Typical Transducer Pair

Table III Transducer Insertion Loss Measurements

	Wafer #	11	13	14	16
LOW FREQUENCY TRANSDUCER	260	59	72	73	64
	280	57	71	72	63
	300	56	67	71	62
	320	55	68	74	60
	340	62	71	77	64
MEDIUM FREQUENCY TRANSDUCER	320	-	84		73
	340	67	79		67
	360	68	84		67
	380	69	74		66
	400	72	77		64
	420	82	82		70
HIGH FREQUENCY TRANSDUCER	420	-			73
	440	81			72
	460	80	>90		75
	480	80			84
	500	76			
	520	82			90

Upon examination of the data presented in Tables II and III it is evident that the low frequency transducer of wafer #11 exhibits significantly lower loss than the other wafers tested. The figure of 56 dB at 300 MHz on the low frequency transducer can be broken down as follows to arrive at a figure for the actual transduction loss of a single transducer. This figure includes 15 dB of mismatch loss as determined from the impedance plot on a network analyzer. In addition, 3 dB of bidirectional loss

exists at both the transmitting and receiving transducer. If these losses are subtracted from the overall 56 dB measured loss figure, the remaining 35 dB represents the propagation loss through the 5 mm path of ZnO which separates the two transducers and the sum of the transduction losses of each device. M. Hamilton[19] of the Air Force Avionics Laboratory has measured the propagation loss of a 290 MHz SAW in ZnO on wafer #3 produced as part of this program. He employed a laser probe technique and measured a value of 40-60 dB/cm. This result has also been supported by the measurements of R.W. Weinert[20] at the Westinghouse Research and Development Center, who reports a loss of 73 dB/cm measured on the intermediate frequency transducer of wafer #6 at 380 MHz. Since the propagation loss is expected to increase as the square of the frequency, Hamilton's 40 dB/cm result would be expected to increase to 69 dB/cm at 380 MHz, which agrees within experimental error with Weinert's value. If we therefore attribute a minimum of 19 dB loss due to propagation through the 5 mm path of ZnO, the remaining 16 dB represents a transduction loss of 8 dB per transduction.

It will be shown in Section 3.5 that approximately 5.0 dB of the measured 7.5 dB mismatch loss suffered at the input transducer is retrievable through the use of a properly designed three element matching network. We would therefore expect to observe a transduction loss of 10.5 dB for the matched transducer.

The other wafers listed in Tables II and III have insertion loss measurements which are significantly greater than those of wafer #11. The mean value for the nine transducers tested at the 300 MHz center frequency of the low frequency transducer is approximately 70 dB. If we again subtract the mismatch, bidirectional and propagation losses we

are left with a value of 14.5 dB for the transduction loss of a single transducer. Including the dissipation in the matching network would increase this figure to approximately 17 dB.

In the case of the intermediate frequency transducer of wafer #11 at its center frequency of 380 MHz, the measured two way insertion loss given in Table III is 67 dB. Using Weinerts[20] propagation loss measurement of 72 dB/cm, made on this wafer, together with the matching data shown in Table V the transduction loss is found to be 5.5 dB per transducer.

Measurements of propagation loss in the ZnO on wafers #11 and 16 were made following those results previously reported and agreed to within experimental error with the results previously obtained independently by Hamilton on wafer #3 and by Weinert on #6. In addition, Weinert made propagation loss measurements in the 7059 glass waveguide deposited on wafer #11 and obtained a value of 4 dB/cm at 245 MHz.

3.5 Matching of ZnO Transducers

The measured impedances and Q factors for eight of the transducer arrays fabricated during the course of this program were listed in Table I of Section 3.3. These highly reactive impedances necessitate the employment of a broadband matching network for each of the individual transducers on a wafer. Wafers #11 and #16 were selected as the two arrays to be matched because #11 was the best sample produced during the program and exhibited the highest Q while #16 exhibited a relatively low Q but still had relatively good acoustical transduction properties. This latter wafer was matched using a series inductance cascaded with a short section of transmission line as shown in Figure 25. Referring to the Smith Chart shown in Figure 26, the original impedance (sweep 1) is resonated by the inductance L_1 to produce sweep 2. The transmission line

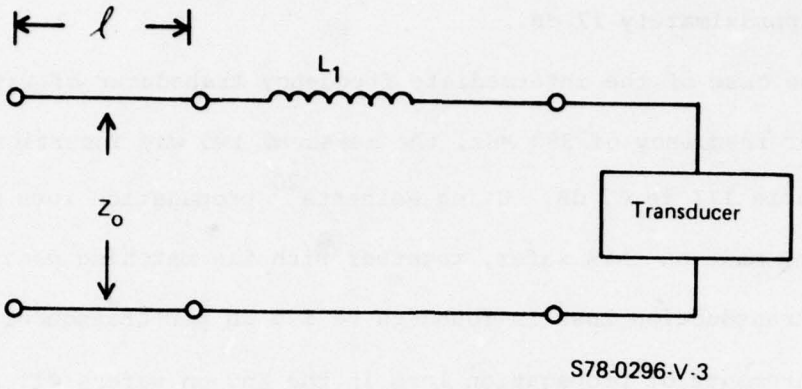

Figure 25 Two Element Low-Q Matching Network

appears as a down-transformer which pulls sweep 3 inside the design VSWR circle. This transformation could also have been performed directly by utilizing an rf transformer. Figures 27 a,b and c show the network analyzer traces of the low, medium and high frequency transducers on this wafer after they have been matched into a 3:1 or less VSWR circle. Table IV summarizes the matching parameters for these low-Q transducers on wafer #16.

In the case of wafer #11 the Q values were significantly higher than those of wafer #16 or of any of the other wafers produced. The correspondingly greater impedance excursions rendered this the most difficult wafer to match, and three element matching networks,as pictured in Figure 28, had to be used to achieve matching of all three transducers on this wafer. The effect of the matching elements on the impedance is depicted on the Smith Chart of Figure 29. The initial impedance, at point 1, is resonated via the series inductor L_1 to obtain the sweep of curve 2. Because of the high unmatched transducer Q, this impedance excursion is very broad, resulting in a high VSWR and significant mismatch loss at the frequency extremes.

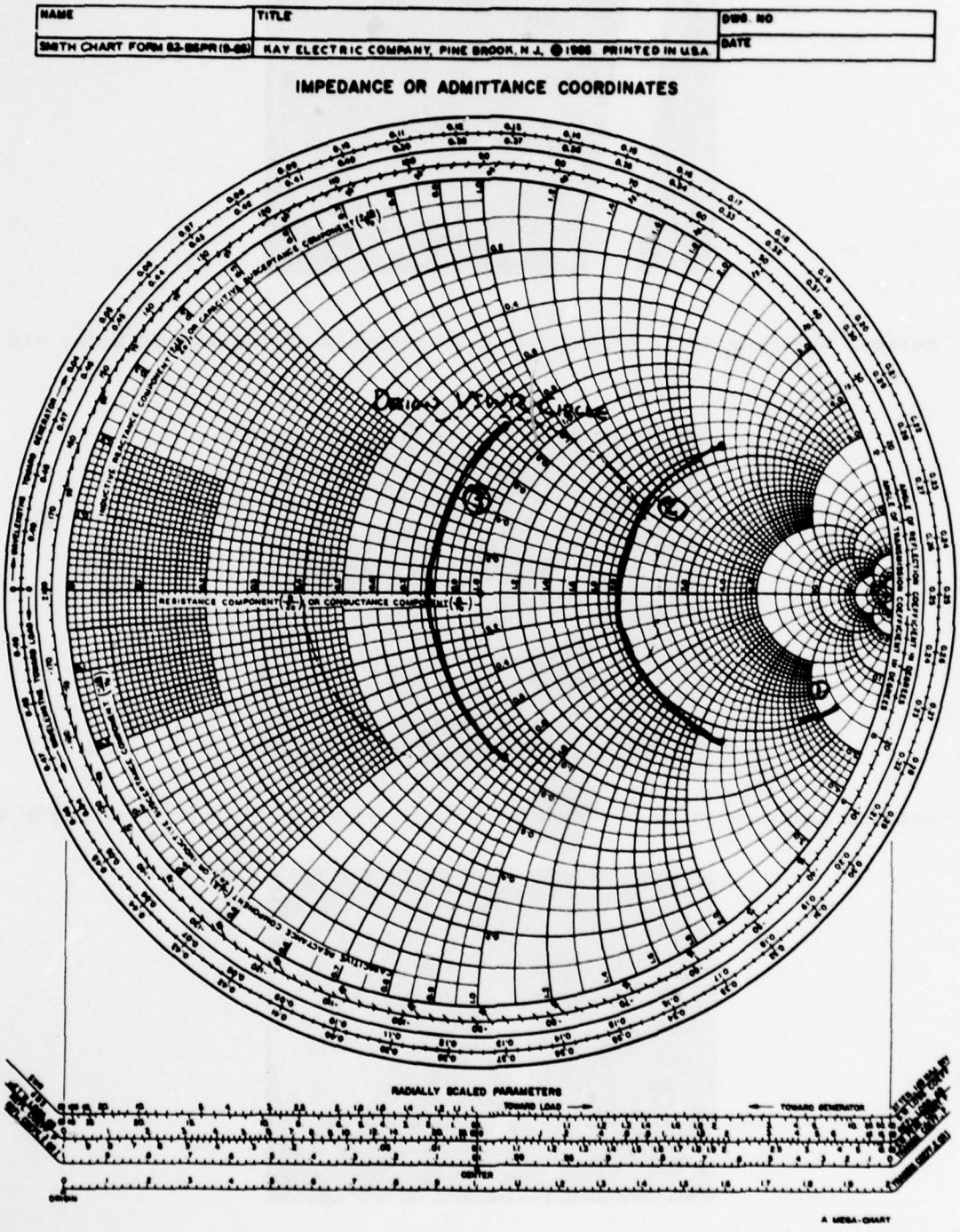

Figure 26 Matching of Low Q Transducer

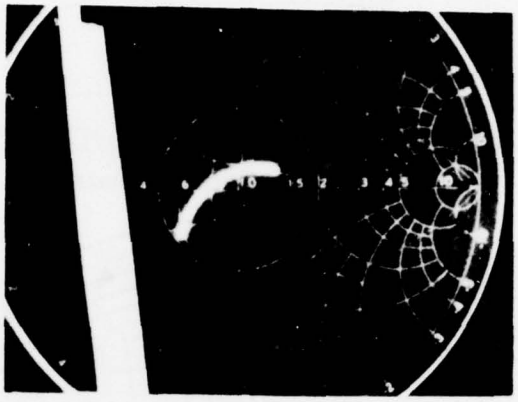

(a) Network Analyzer Trace of Matched Low Frequency Transducer of Wafer #16

(b) Network Analyzer Trace of Matched Medium Frequency Transducer of Wafer #16

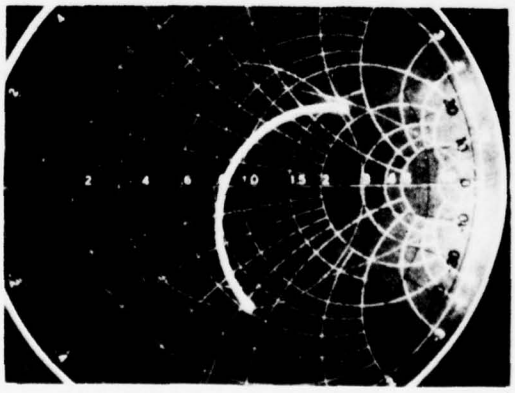

(c) Network Analyzer Trace of Matched High Frequency Transducer of Wafer #16

Figure 27

Table IV Matching Parameters for the Low-Q Transducers on Wafer #16

Transducer Frequency Range, MHz	Unmatched Average Impedance, ohms	Unmatched VSWR	Unmatched Loss Due To Mismatch, dB	L_1, nH	Maximum Matching VSWR	Maximum Final Mismatch Loss, dB *	(Initial Mismatch Loss) -(Final Mismatch Loss), dB
264-336	112-j285	17:1	6.8	130	2:1	1.5	5.3
336-432	87-j279	19:1	7.2	100	2.5:1	1.9	5.3
432-550	51-j253	29:1	8.9	60	3:1	2.3	6.6

* Includes an estimated 1.0 dB matching component loss

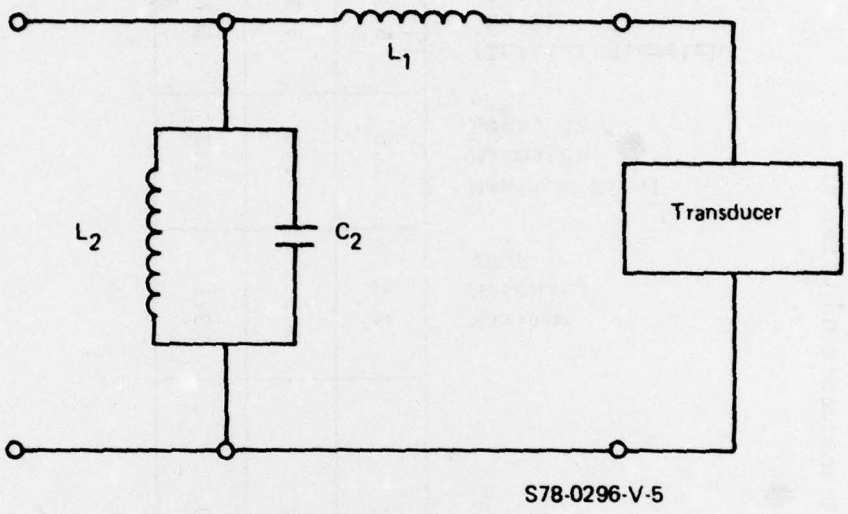

Figure 28 Three Element High-Q Matching Network

The inductor L_2 and capacitor C_2 form a shunt-shunt resonance which wraps the broad sweep inside a constant VSWR circle so that the broadband mismatch loss is less than or equal to the loss corresponding to the constant VSWR perimeter.

Figures 30 (a) and (b) show the low frequency transducer resonated first to the real axis of the Smith Chart with the impedance L_1 and then wrapped with L_2 and C_2 over the 24% fractional bandwidth. Figures 31 (a) and (b) and 32 (a) and (b) show the same results on the medium and high frequency transducers, respectively. The degree or "tightness" of wrap, which is controlled by the values of L_2 and C_2, varies in these three cases. All of the elements were adjusted to yield as small a constant VSWR boundary as possible. The constant VSWR = 2.5:1 circle is shown for reference in

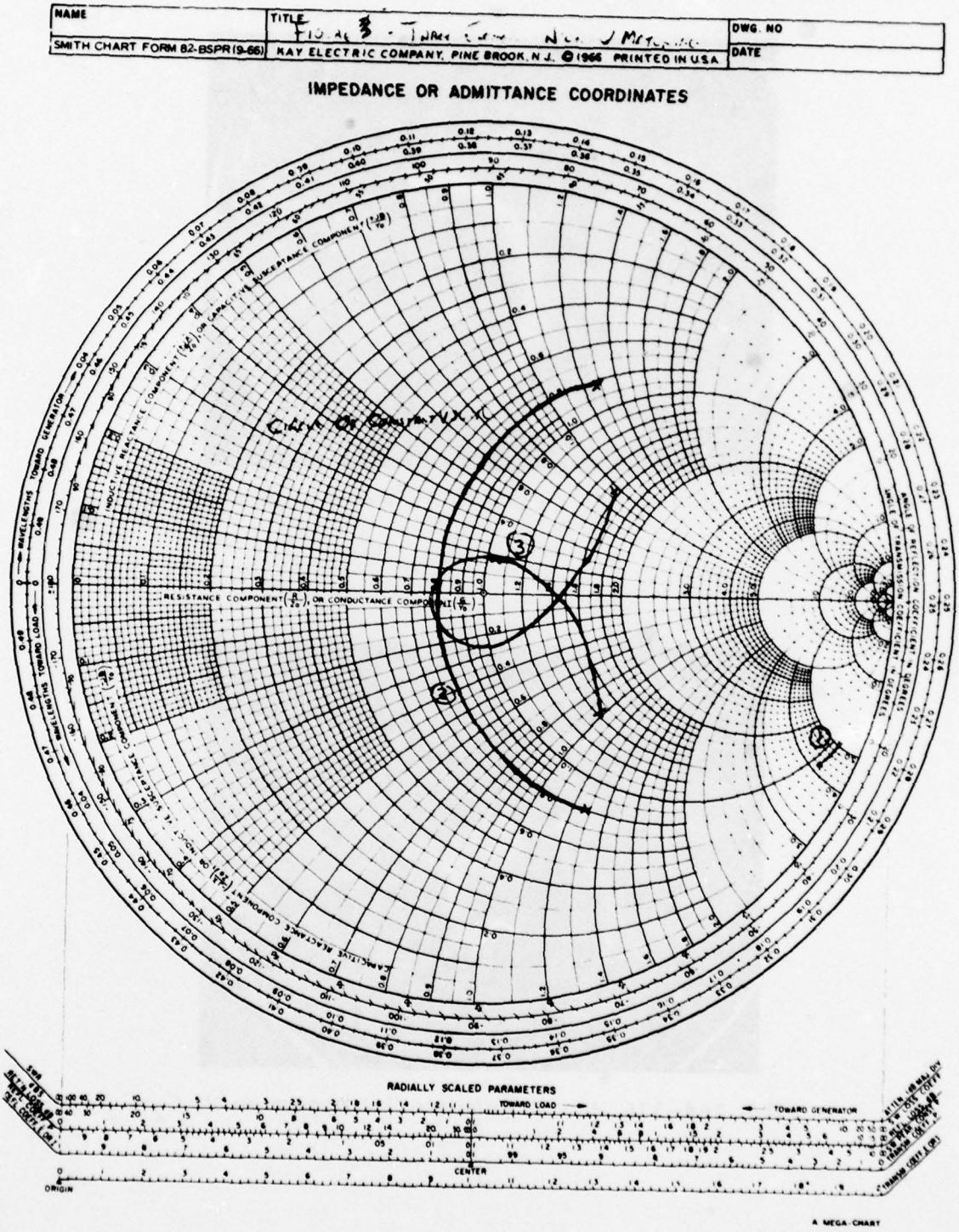

Figure 29 Matching of High Q Transducer

(a) 264-336 MHz Transducer Resonated with L_1

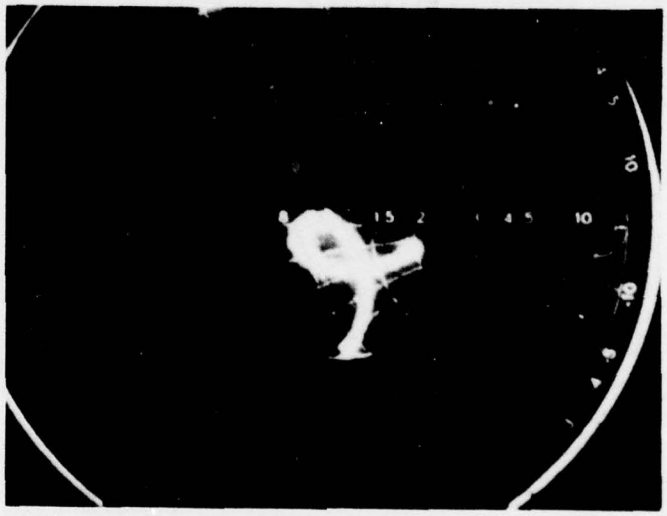

(b) 264-336 MHz Transducer Wrapped with L_2-C_2

Figure 30 Transducer Impedances Measurements (Wafer #11)

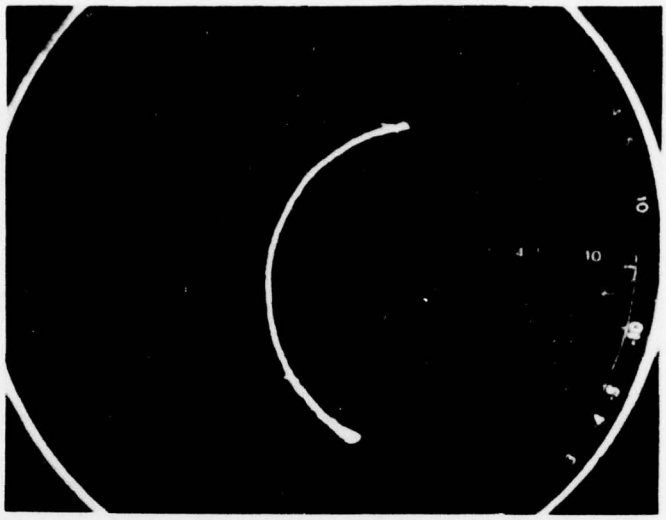

(a) 336-432 MHz Transducer Resonated with L_1

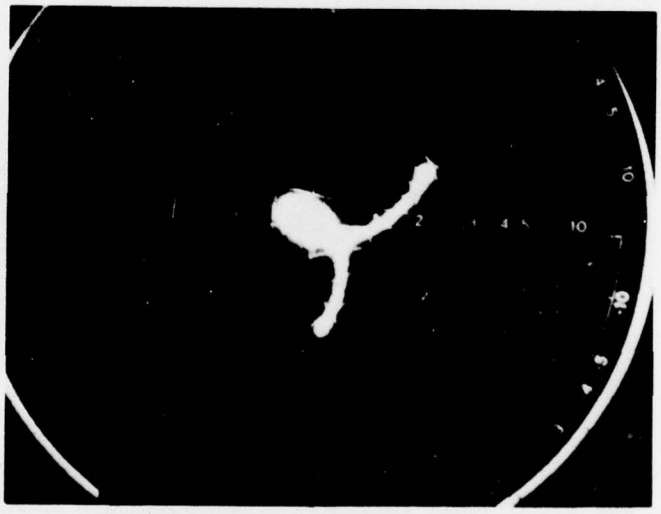

(b) 336-432 MHz Transducer Wrapped with L_2 - C_2

Figure 31 Transducer Impedances Measurements (Wafer #11)

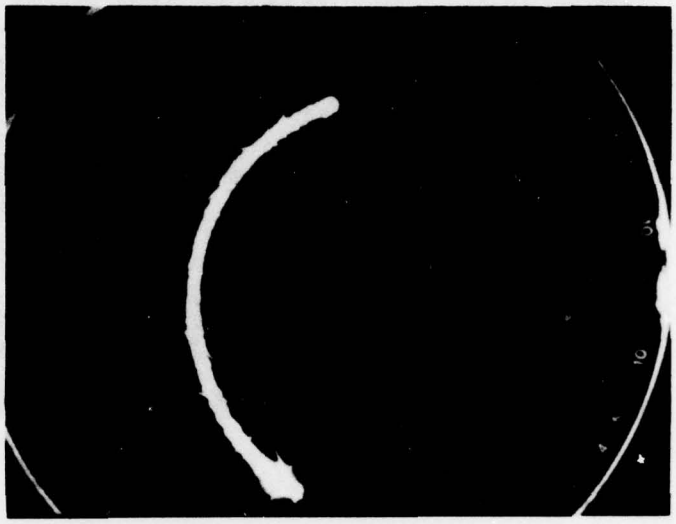

(a) 432-550 MHz Transducer Resonated with L_1

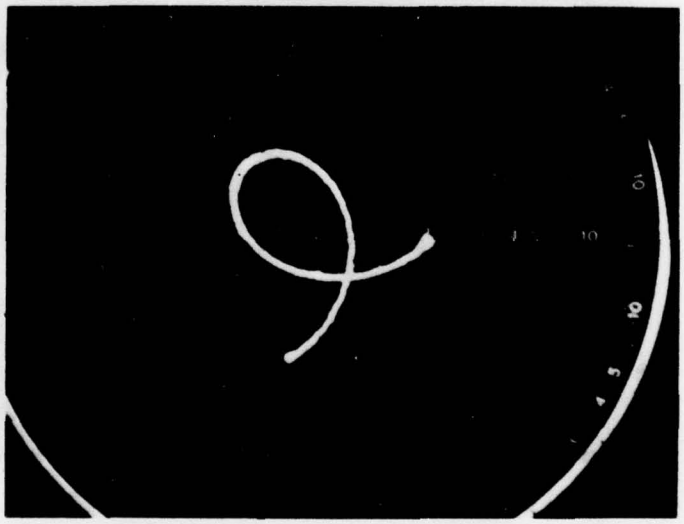

(b) 432-550 MHz Transducer Wrapped with L_2 - C_2

Figure 32 Transducer Impedances Measurements (Wafer #11)

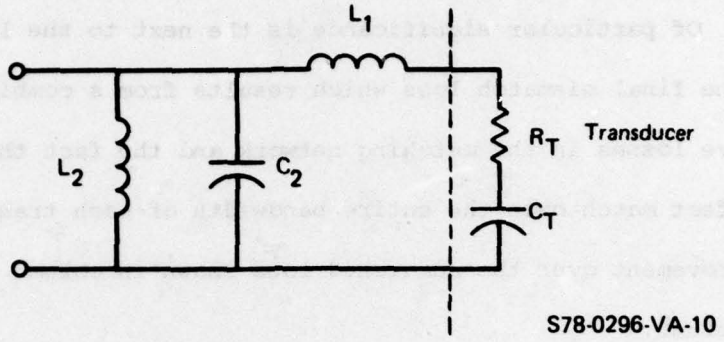

(a) Three-Element High-Q Matching Network

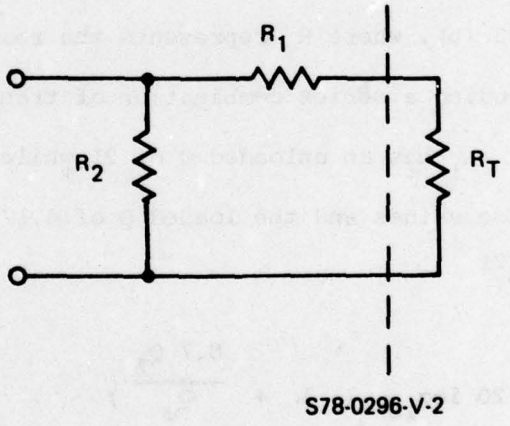

(b) Approximate Equivalent Circuit for Dissipation Estimation

Figure 33

each of the network analyzer traces.

Table V summarizes the matching parameters for the high Q transducers on wafer #11. Of particular significance is the next to the last column which shows the final mismatch loss which results from a combination of the dissipative losses in the matching network and the fact that we do not achieve a perfect match over the entire bandwidth of each transducer. The resulting improvement over the unmatched loss shown in column 4 is presented in the last column.

In order to estimate the dissipative losses in the matching networks, we consider the network configuration shown in Figure 33 (a). The dissipative loss in the capacitor is very much smaller than that in either of the inductive elements throughout the matching bandwidth, and it can be neglected. We can thus reduce the circuit for the purpose of dissipation estimation to that shown in Figure 33 (b), where R_T represents the real part of the transducer impedance including a series combination of transducer resistance and radiation resistance. L_1 has an unloaded Q of 21 while the unloaded Q of L_2 is 35. Using these values and the loaded Q of 4.17 for a 24% bandwidth in the equation[21]

$$\text{Loss (dB)} = 20 \log_{10} \left(1 + \frac{0.7\, Q_\ell}{Q_u} \right)$$

gives a dissipation loss for each matching network of 1.7 dB.

Table V Matching Parameters for the High-Q Transducers on Wafer #11

Transducer Frequency Range, MHz	Unmatched Average Impedance, ohms	Unmatched VSWR	Unmatched Loss Due to Mis-Match, dB	Matching Component Values			Maximum Matched VSWR	Maximum Final Mismatch Loss*, dB	Initial Mis-Match Loss Final Mismatch Loss, dB
				L_1, nH	L_2, nH	C_2, pf			
264 - 336	59 - j250	20:1	7.5	100	22	15	2.4:1	2.50	5.0
336 - 432	52 - j261	30:1	9.0	60	18	18	2.4:1	2.50	6.5
432 - 550	28 - j238	40:1	10.5	60	5	18	2.15:1	2.33	8.17

* 1.7 dB Matching component loss added

4.0 DISCUSSION OF RESULTS

As shown in Table III of the previous section, wafers #11 and 16 were measured to have transduction loss figures well below those of other wafers prepared during the course of this program. After correction for bidirectional loss, mismatch loss and acoustic propagation loss in the ZnO, the low frequency transducer on wafer #11 was found to have a transduction loss of only 8 dB. By proper impedance matching it is possible to operate this transducer at a transduction efficiency of -10.5 dB, considerably better than the -14 dB goal for this program. The corresponding value for the low frequency transducer on wafer #16 is 10.4dB, which is also well within the stated goal.

Likewise, the intermediate frequency transducer on both wafer #11 and #16 provide figures of 7.5 dB and 7.4 dB, respectively, while the high frequency transducers yield values of 6 dB and 4.1 dB, respectively. All of these figures, which are significantly better than the program goals, are based upon measured values of the mismatch and insertion losses. The propagation loss was originally obtained by utilizing the measurements of Hamilton[19] taken at 290 MHz and those of Weinert[20] taken at 380 MHz and assuming a frequency square dependence to extrapolate the results to other frequencies. This technique was subsequently justified on the basis of propagation loss measurements made by Weinert on wafers #11 and 16 at a series of frequencies very near those at which the insertion loss measurements were made. These latter measurements eliminate the possibility that the propagation loss was lower on those wafers exhibiting lower total insertion loss.

Attempts to determine the value of the electromechanical coupling coefficient, k^2, from the expression[11]

$$k^2 = 4C\ f\ R_a$$

where C is the capacitance per finger pair and R_a the radiation resistance are confused by the inability to accurately determine R_a. Based upon theoretical calculations of dissipative resistance, R_D, as well as on high frequency impedance measurements it would appear that R_a is small compared to R_D. If k^2 is to have a value which is near its maximum value of 0.027,[9] R_a should have a value of 47.5 ohms. Since the real part of the transducer impedance for the low frequency transducer on wafer #11 has been determined to be 59 ohms and since it corresponds to the series sum of R_a and R_D, it is unlikely that the value of R_a is nearly as great as 47.5 ohms. As a result, we appear to have a discrepancy between the excellent results measured on the transduction loss and the value of k^2 calculated from the impedance results. This problem is still unresolved at this time.

The ability to fabricate transducers exhibiting transduction losses of less than 10 dB holds great promise for ZnO/silicon-based integrated optics technology. On the other hand, the yield on high-quality ZnO wafers appears to be of the order of 10%, and it does not appear to be possible to characterize the transducer quality on the basis of inspecting the ZnO film. All of the wafers for which data have been provided in Section 3 appear perfectly clear and uniform under visual or microscopic inspection, yet great variations in transducer performance were observed. The electrical Q of the transducer also does not appear to be a positive

criterion which may be utilized to sort the transducers, since one of the best wafers produced has high Q's while the second good wafer has Q's which are lower than those of other transducers that were far more lossy. Consequently, it is necessary to complete the fabrication of the device and subsequently characterize the transducers on the basis of their measured acoustical properties.

Still another problem area associated with this technology involves the very high propagation losses measured in the piezoelectric material by two separate investigators. M.C. Hamilton[19] has measured a propagation loss of 40-60 dB/cm at 290 MHz while R. W. Weinert[20] has measured losses of 73 dB/cm at 380 MHz on wafer #6, 78 dB/cm at 382 MHz and 118 dB/cm at 484 MHz on wafer #16, and 50 dB/cm at 280 MHz and 115 dB/cm at 480 MHz on wafer #11. These measurements made by two different investigators on four different wafers are sufficiently close to the expected f^2 dependence of propagation loss to support each other, and to point out the difficulties which will arise at still higher frequencies as the need for increased bandwidth forces operation at frequencies in excess of 1 GHz. Nevertheless, the results of this program do suggest that if the yields can be improved and if the transducers can be designed such that the SAW path in the piezoelectric is short, silicon-based integrated optics may prove advantageous at least for applications which do not demand extremely wide bandwidths.

REFERENCES

1. M.C. Hamilton, Private Communication

2. M. Gottlieb, Private Communication

3. G. Marx, M. Gottlieb and G.B. Brandt, "Integrated Optical Detector Array, Waveguide and Modulator Based on Silicon Technology," IEEE J. Solid State Circuits, SC-12, 10, (1977).

4. J.T. Boyd and C.L. Chen, "An Integrated-Optical Waveguide and Charge-Coupled-Device Image Array," IEEE J. Quantum Electronics, QE-13, 282, (1977).

5. J. de Klerk, "A Physical Approach to Elastic Surface Waves" from "New Directions in Physical Acoustics," LXIII Corso, Soc. Italiana di Fisica, Bologna, Italy, 1976.

6. J.F. Nye, Physical Properties of Crystals, Clarendon Press, Oxford, England, 1957.

7. J.J. Campbell and W.R. Jones, A Method for Estimating Optimal Crystal Cuts and Propagation Directions for Excitation of Piezoelectric Surface Waves," IEEE Trans. Sonics and Ultrasonics SU-15, 209 (1968).

8. A.J. Slobodnik, R.T. Delmonico and E.D. Conway, Microwave Acoustic Handbook, Vol. 2, AFCRL-TR-74-0536, Air Force Cambridge Research Labs (1974).

9. L.P. Solie, "Piezoelectric Waves on Layered Substrates", J. Appl. Phys. 44, 619, (1973).

10. W.R. Smith, H.M. Gerard, J.H. Collins, T.M. Reeder and H.J. Shaw "Analysis of Interdigital Surface Wave Transducers by Use of an Equivalent Circuit Model," Trans. IEEE, MTT-17, 856 (1969).

11. G.S. Kino and R.S. Wagers, "Theory of Interdigital Couplers on Nonpiezoelectric Substrates", J. Appl. Phys., 44, 1480, (1973).

12. C.S. Tsai, "Wideband Guided-Wave Acoustooptic Bragg-Devices and Applications" Proc. 1975 Ultrasonics Symp. IEEE Cat. 75, CH0-994-4SU, 120, (1975).

13. B. Kim and C.S. Tsai, "High Performance Guided-Wave Acoustooptic Scanning Devices Using Multiple Surface Acoustic Waves," Proc. IEEE, 64, 788, (1976).

14. C.S. Tsai, L.T. Nguyen, and B. Kim, "Wideband Guided-Wave Acoustooptic Bragg-Diffraction Using Phased-Surface Acoustic Wave Array in $LiNbO_3$ Waveguides", Proc. 1975 Ultrasonics Symp. IEEE Cat. 75, 42, (1975).

15. F.S. Hickernell and J.W. Brewer, "Surface-Elastic-Wave Properties of dc-Triode Sputtered Zinc Oxide Films," Appl. Phys. Lett., 21, 389, (1972).

16. H.W. Bode, Network Analysis and Feedback Amplifier Design, D. Van Nostrand Co., New York, 1945.

17. R.M. Fano, "Theoretical Limitations on Broadband Matching of Arbitrary Impedances", Journ. of the Franklin Institute, 249, 57, (1950).

18. I.A. Vikrovov, Rayleigh and Lamb Waves, Plenum Publishing Co., New York, 1967.

19. M.C. Hamilton, Private Communication

20. R.W. Weinert, Private Communication

21. D.R.J. White, A Handbook on Electrical Filters; Synthesis, Design, and Applications, Germantown, MD: D.R.J. White, 1963, p. 193.

☆U.S.Government Printing Office: 1978 — 657-002/262